WASHINGTON UNIVERSITY

THE HENRY EDWIN SEVER GRADUATE SCHOOL

DEPARTMENT OF CIVIL ENGINEERING

THE DEVELOPMENT OF FRAGILITY RELATIONSHIPS

FOR CONTROLLED STRUCTURES

by

Ellen Taylor

Prepared under the direction of Professor Shirley J. Dyke

A thesis presented to the Henry Edwin Sever Graduate School of

Washington University in partial fulfillment of the

requirements for the degree of

MASTER OF SCIENCE

May 2007

Saint Louis, Missouri

WASHINGTON UNIVERSITY

THE HENRY EDWIN SEVER GRADUATE SCHOOL

DEPARTMENT OF CIVIL ENGINEERING

ABSTRACT

THE DEVELOPMENT OF FRAGILITY RELATIONSHIPS

FOR CONTROLLED STRUCTURE

by

Ellen Taylor

ADVISOR: Professor Shirley J. Dyke

May 2007

St. Louis, Missouri

To mitigate the dynamic effects of earthquakes in structures, several response modification strategies have been developed, including implementation of passive, active, and semiactive devices. Structures with mitigation devices have shown to reduce the responses during large earthquake events. Although recent studies on controlled structures have mainly focused on modeling, performance and control strategies, a systematic study on the vulnerability of controlled structures has not been conducted. Since earthquakes can be catastrophic events, seismic risk assessments are becoming more valuable to mitigate future loss. A fragility analysis is the conditional probability of a system meeting or exceeding a specified performance limit state given the occurrence of a particular demand and is decoupled from the probability of the occurrence of the demand. A fragility relationship helps determine the risk of structures and to compare possible strategies to reduce the likelihood of structural damage. Performance limits can range from immediate occupancy to collapse prevention while using a range of earthquake demands. This thesis will focus on formulating a methodology for generating fragility functions for controlled structures to more easily depict the reduction of probability of failure compared to a structure without devices.

To my friends and family who have continually supported me.

Contents

List of Tables

List of Figures

Acknowledgements

I would like to thank my advisor Dr. Shirley Dyke for her time and guidance during the preparation of this thesis, as well as thank Oh-Sung Kwon and Naru Nakata at the University of Illinois Urbana-Champaign for their technical assistance using UI-SIMCOR and ZeusNL. I would also like to thank Dr. Thomas Harmon and Dr. Phillip Gould for their time to serve on my defense committee.

<div align="right">

Ellen Taylor

</div>

Washington University in St. Louis

May 2007

Chapter 1

Introduction

To protect civil structures from severe damage, structural control has become an attractive means to mitigate responses from severe earthquake events. Several types of structural control have been proposed and studied, including passive, active, and semiactive systems. In a passive control strategy, device forces are developed from structural motions. Although passive devices have been shown to reduce the responses and require no power, passive devices cannot adapt to changes in usage or loading to the structure. Active systems respond to measured responses using sensors placed on the structure offering potential performance gains. Semiactive systems combine the benefit of changing control characteristics of active systems with the benefit of stability of passive systems. Semiactive devices can only dissipate energy to a system and, therefore, are very reliable, stable systems.

The damaging effects of earthquakes include loss of human life, property damage and business interruption. Engineers are starting to use performance based design approaches to design a structure to resist an acceptable level of damage. However, today's building codes focus mainly on ensuring life safety. Structures meeting code requirements are still vulnerable in severe earthquake events. Structural control is an innovative way to ensure the responses remain below a prescribed level and to decrease the vulnerability of the system.

Seismic risk assessments are an effective way to assess the vulnerability of structure to mitigate future losses. Fragility assessments play an important role in a seismic risk assessment by analyzing the response and probable damage of structures to provide loss

estimation and aid in decision making (Wen and Ellingwood 2005). A fragility analysis is less complex, less costly, and more easily understood by decision makers than a complete risk assessment. Seismic fragilities can be broadly defined or redefined as needed to assess consequences by accounting for various structural characteristics and on the extent of rehabilitation (Wen, Ellingwood and Bracci 2004).

This thesis will present a method to develop a fragility curve for a controlled structure. Motivation for this research and a literature review is presented in this chapter.

1.1 New Madrid Seismic Zone

The largest known earthquake in the contiguous United States occurred along the New Madrid Fault in central Mississippi Valley in 1812. The soil conditions in this area cause the damaging effects of earthquakes to be felt at greater distances than typical earthquakes in areas on the west coast. In recent years, scientists and geologists have discovered evidence of other previous large earthquakes in this area. Therefore, strong earthquakes will continue to be a threat to the Midwest. Fortunately, the Mississippi Valley was scarcely populated in 1812, but now a major earthquake could potentially cause great devastation in many major cities in the Midwest including Memphis, Tennessee and St. Louis, Missouri (Stover and Coffman 2006). Scientists, geologists, and engineers are working together to minimize the consequences of future earthquakes through various seismic risk reduction strategies.

The Mid-America Earthquake (MAE) Center is one of three national earthquake engineering research centers established by the National Science Foundation to investigate new approaches to seismic risk assessment and mitigation through interdisciplinary research and is taking the lead in regional loss assessment modeling and characterization of earthquake hazard in the central US. The MAE Center has

developed a new consequence-based approach that incorporates estimating seismic vulnerability across networks and identifying seismic hazards.

1.2   Consequence Based Engineering

MAE Center researchers have coined a new term for a new seismic risk reduction strategy called consequence-based engineering (CBE) and defines it as:

> Consequence-based engineering is a new paradigm for seismic risk reduction across regions or systems that incorporates identification of uncertainty in all components of seismic risk modeling and quantifies the risk to societal systems and subsystems enabling policy-makers and decision-makers to ultimately develop risk reduction strategies and implement mitigation actions. (Abrams, Elnashai and Beavers 2002)

Practicing engineers can use this method as outlined in Figure 1.1 to identify possible consequences of seismic hazards. The flowchart is divided into four categories: rapid assessment, decision making, damage synthesis, and consequence minimization. Preliminary analyses are performed during the rapid assessment stage for a quick assessment of the system using inventory or pre-existing data. The decision making process includes determining if the consequences are acceptable, if acceptable consequences should be redefined, if a more detailed analysis should be performed, and if interventions should be considered. Parameters can be refined for the system if a further analysis is necessary. One important step in the damage synthesis process is refining fragility relations. Approximate vulnerability functions are used to quickly estimate losses, but building specific fragility functions are often needed to assess consequences by accounting for specific structural characteristics. The benefits of retrofitting an individual structure (such as a hospital or fire station) that is an integral part of the system can be shown through a detailed fragility analysis of a single structure. CBE aims at quantifying and minimizing consequences across specific regions through a step-by-step process, and the overall effect of various system intervention strategies

such as retrofitting a specific structure can be investigated to minimize consequences to an acceptable level (Abrams, Elnashai and Beavers 2002).
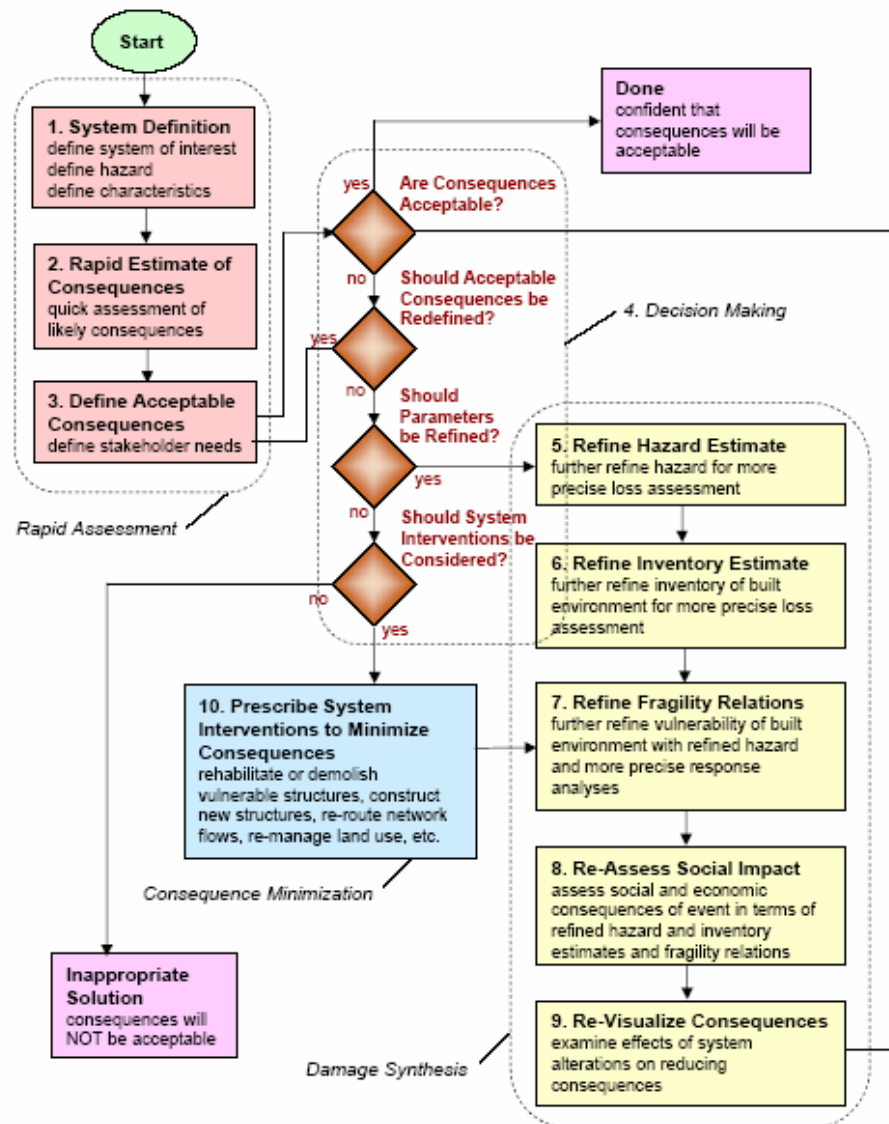
Figure 1.1 Consequence Based Engineering Paradigm after Abrams, Elnashai and Beavers 2002

To minimize consequences to a system, the main contributors of risk should be the focus of further investigation through a probabilistic safety assessment. A probabilistic safety assessment (PSA) is an important component to the CBE framework by focusing on why and how systems might fail while explicitly treating uncertainty. PSA is a

methodology to evaluate risk by evaluating the severity of the possible loss from a particular hazard and the probability of the hazard occurring. A limit state, or a condition at which a system does not perform to a desired level, is defined. The fully coupled risk assessment includes both the probability of the hazard and the conditional probability of the system attaining the prescribed limit state. For a seismic assessment, the hazard is defined as ground motion excitations. The conditional probability is the fragility of a component or system and is an integral part of a PSA (Wen, Ellingwood and Bracci 2004).

1.3   Fragility Curves

For a full seismic risk analysis, analyses of both the occurrence of the ground motion intensity level and the fragility of the system are necessary. Although a full PSA is sometimes necessary, the results of a fragility assessment are particularly helpful for decision-making. Fragility is defined as the conditional probability of a system or component meeting or exceeding a prescribed performance limit state given the occurrence of a particular demand or hazard. Advantages of a fragility analysis over a fully coupled risk analysis include being uncoupled from the hazard analysis, avoiding interpretation of small limit states, being less complex and costly, and involving fewer disciplines than a fully coupled risk analysis. A fragility analysis does not consider the occurrence of the hazard which may also be considered during decision-making. However, a fragility analysis is often more easily understood for decision makers with a limited technical background since knowledge of the hazard recurrence interval is not necessary (Wen, Ellingwood and Bracci 2004).

Recently MAE Center researchers have proposed a loss estimation framework that maps damage states to the performance levels used to develop fragility curves. The mean value of total damage can be found to compare the expected total damage as a function of spectral acceleration. This probabilistic approach allows uncertainty to be

quantified and confidence and prediction bands to be developed (Bai, Hueste and Gardoni 2006).

The need for new methodologies to develop fragility relationships for various types of structures and retrofit strategies is clear when considering the CBE framework. Many researchers have developed methods to determine the relationship between the ground motion intensity level and the response of the structure. Shinozuka et al. (2000a) presented both empirical and analytical fragility curves using a two-parameter lognormal distribution function. Empirical fragility curves require damage data associated with past measured earthquakes which is often scarce or too small of a sample size for an accurate analysis. Singhal and Kiremidjian (1996) first presented a Monte Carlo-simulation approach for analytical fragility curves and then followed up on this work by presenting a Bayesian method to combine building damage data with analytical fragility curves for a more robust fragility analysis (Singhal and Kiremidjian 1998).

Generalized fragility relationships are often used for a rapid assessment. Jeong and Elnashai (2004) have developed an approach to derive a fragility curve using only three parameters of a structural system: stiffness, strength, and ductility. A database of parameterized vulnerability functions has been created for a quick analysis. Although a class of structures can easily be studied and compared using a parameterized method, further investigation is needed if parameters are needed to be refined during the damage synthesis process of CBE. When a building specific analysis is necessary, various analytical methods can be used to determine a relationship between ground motion severity and structure response for a complete analysis.

1.3.1   Fragility Analysis of a Linear Elastic System

A relationship between the system response and the intensity measure is easily modeled for a system that stays within the linear range. A linear structural static or dynamic

analysis can determine the design seismic forces and the resulting displacements. The application of the principle of modal superposition makes the relationship between the response of the system and the earthquake demand easy to determine. For small earthquake intensity levels, a linear analysis could be an appropriate method, but is not an accurate method if the structure enters the inelastic range (Bai 2004).

1.3.2   Fragility Analysis of a Nonlinear Inelastic System

For moderate to severe earthquake intensity levels, a structure rarely remains in the linear elastic range. Nonlinear behavior of the system is often observed. A nonlinear analysis is a more accurate method to determine the relationship between the responses of the system and the ground motion intensity level, but modal superposition is no longer valid for a nonlinear system. The most accurate approach is to use a nonlinear dynamic analysis using specific ground motion records (Wen, Ellingwood and Bracci 2004; Bai 2004; Shinozuka et al. 2000a; etc.). Time history analyses using previously recorded earthquakes records or synthetic ground motions are used to determine the relationship between structural responses and earthquake intensity levels. Due to the nonlinear nature of the analysis, responses from more than one earthquake record should be used. Intensity levels from low to high should be used to cover a range of structural response demands (Wen, Ellingwood and Bracci 2004).

Shinozuka et al. (2000a) examined the potential of using a nonlinear static procedure using the capacity spectrum method. The results of the capacity spectrum method that utilizes a pushover curve was shown to be very similar to results using a nonlinear time history analysis for minor damage, but when major damage resulted, large errors existed between the two methods. Lew and Kunnath (2002) also showed the results from a nonlinear static analysis did not give a good estimate of interstory drift when compared to a nonlinear dynamic analysis. However, results from a pushover curve are often used

to determine member specific limit states such as first yield (Wen, Ellingwood and Bracci 2004).

1.3.3   Fragility Curves and Retrofitting

Using today's design codes, structures are designed to meet life safety standards. However, older structures suffer from deterioration and many structures in the mid-America region were not even designed with due consideration to earthquake loads. To minimize the possibility of devastation from an earthquake in the region, engineers and policy makers are investigating different retrofitting strategies for structures that are an important component to a community's infrastructure.

Many MAE Center researchers have studied various static retrofitting strategies for buildings and bridges. Wen, Ellingwood and Bracci (2004) presented a report for vulnerability functions for consequence-based engineering that included fragility curves for retrofitted reinforced concrete frame structures and steel building frames. Bai (2004) investigated various retrofitting strategies including the addition of shear walls, column jacketing, and confinement of column plastic hinge zones for a five-story reinforced concrete building. Fragility relationships for retrofitted bridges have also been developed by Kim and Shinozuka (2004) and Padgett and DesRoches (2006).

1.4   Structural Control

Structures are typically designed considering only static loading conditions. However dynamic loads continually occur over the lifetime of the structure. Because dynamic loads can lead to fatigue and failure, engineers try to reduce the vibrational effects from dynamic loads such as winds, earthquakes, blasts, people walking, or machinery. The devastation from recent earthquakes such as the Northridge earthquake in 1994 and the Kobe earthquake of 1995 has motivated engineers and scientists to investigate new

mitigation techniques to enhance structural functionality and safety against natural and manmade hazards (USGS 2006). Structural control is applying modern control strategies to civil engineering structures to reduce structural responses during severe dynamic events. The idea of structural control was first proposed in the US in 1972 by Yao and now researchers from around the world are continually investigating and inventing new control strategies for civil engineering. Passive, active, and semiactive systems are the three main categories of structural control with hybrid systems becoming a new method to combine passive and active or semiactive systems.

Passive strategies are the most widely accepted by the engineering community. Passives systems use the structure's responses to dissipate vibrational energy. Advantages of passive systems include no necessary external power requirements, no necessary sensors or computational power, and their inherit stability. Base isolation is the most commonly designed passive system, but other passive systems including tuned mass dampers, passive braces, and sliders have also been investigated and implemented. Taipei 101, the world's largest building with respect to highest occupied floor as of 2006, employs a tuned mass damper to dissipate vibrations from winds and earthquakes. Gilani, Miyamoto, and Kohagura (2006) implemented fluid viscous dampers in a hospital and a police headquarters in California to retrofit the essential facilities to a target level of performance. However, passive devices are unable to adapt to structural changes and changing environments, which has led to further research in other classes of controlled structures.

Active, semiactive, and hybrid systems integrate real-time controllers and sensors within the structure to form a smart structural system and therefore have shown improved performance over passive systems. Shooshtari and Saatcioglu (2006) have also shown the potential for up to 60% reduction in interstory drift by implementing an active system in a reinforced concrete building. Active systems use actuators to supply external energy to the system and sensors to determine appropriate control action from the responses of the structure. Research on control algorithms for active and semiactive

systems are continually being researched to improve the performance of such systems. Kitagawa and Akutagawa (2006) showed that a hybrid control system with optimal fuzzy control was effective for the nonlinear behavior of a structure. Acceleration feedback control algorithms are often used for active and semiactive control systems because full state feedback is often difficult to implement (Dyke et al. 1996b). Active and semiactive systems rely on external power, but power outages are common during severe earthquake events. Williams (2004) investigated fault tolerant design in active and semiactive systems and determined that when those systems act as passive fail-safe systems, structural responses are still reduced when compared to the original structure without control. The potential for increase performance over passive control without the concerns of large energy requirements and stability has led many researchers to focus their attention on semiactive control (Dyke, et al. 2005).

1.5   Objective and Scope

The performance and reliability of controlled systems have been studied by numerous researchers around the world, but the vulnerability of controlled structures should also be considered by those making recommendations and decisions regarding retrofit or design options. Thus, fragility of controlled systems is a new interest for engineers, building owners, and policy makers. The objective of this research is to present a methodology to develop fragility curves for controlled structures. The research presented in this thesis is part of EE-1 Vulnerability Functions MAE Center Project to develop procedures for the formulation of relationships between ground motion severity and the probability of a set of limit states being reached and for the reduction of loss from different intervention approaches (http://mae.ce.uiuc.edu). MAE Center researchers have recently studied multiple retrofit options to strengthen structures including the addition of shear walls, braces, and column jackets to reduce the vulnerability of the system. This thesis investigates the addition of control devices as a retrofit option to be included in the database of possible retrofit options for the EE-1

project. Passive and active systems are considered in this study, but the advantages of semiactive and hybrid systems will direct future investigations into the vulnerability of these classes of controlled structures.

The general methodology to develop a fragility curve along with the software selection and modeling of passive and active systems are discussed in Chapter 2. Chapter 3 gives the description of the steel moment-resisting building model used for the study and the uncontrolled fragility of the model. Uncertainty within the fragility analysis is discussed in Chapter 4. Fragility curves for a passively and actively controlled structure are presented in Chapter 5 and Chapter 6, respectively, along with a comparison of two device configurations. Chapter 7 summarizes the research and presents recommended future investigations.

Chapter 2

Background

Although recent studies have shown that vulnerability relationships provide an effective way to compare retrofit techniques, fragility curves for structures with controlled devices have not been examined. This chapter discusses the five main steps to develop a fragility curve and the appropriate software for a nonlinear analysis, as well as the algorithm development of the passive and active devices.

2.1 Fragility Curves

A fragility relationship (F_R) is the probability of a set of limit states (LS) being reached or exceeded at a prescribed system demand ($D=d$) as defined in Equation 2.1. For a seismic analysis, the system demands are a result of various ground motion severities and the structural performance limit states can vary from immediate occupancy to complete failure. The characteristics of the structure, representative earthquake intensities, and the uncertainty of the capacity and demand are all included in developing a fragility curve (FC). The central location of the FC is determined from the capacity of the system and the slope of the curve is controlled by the uncertainty (Wen et al. 2004). The FC would simply be a step function if the entire system was deterministic and no uncertainty was present in the analysis.

$$F_R(x) = P\big[LS/D = d\big] \tag{2.1}$$

For a rapid evaluation, generalized fragilities of the main components of a system may be used to avoid repetitive time history analyses. However, for a more detailed assessment, individual structures are examined using a complex nonlinear analysis. Five main steps outline the procedure to develop a fragility curve for a nonlinear controlled system:

1. Appropriate ground motions are determined.
2. An analytical model of the controlled structural system is developed.
3. A probabilistic seismic demand model is calculated from time history responses.
4. The capacity of the elements is determined.
5. The fragility curve is developed using an appropriate equation.

Ground motions characteristic of the region of various magnitudes should be used for a more accurate result. Because modal superposition is not applicable to nonlinear systems, a time history response analysis should be performed to calculate a probabilistic demand curve to determine a relationship between the structural response demand and the intensity measure. Limit states are determined to define the capacity of the whole system or elements of the system. Uncertainty of the building model, the power law equation, and the capacity should all be include in the final equation and result. The following sections provide more detail on these steps.

2.1.1   Simulated Ground Motion Records

Ground motion records are used to investigate the correlation between structural response and seismic intensity measures. In areas of high seismicity, such as California or Japan, both small intensity and large intensity earthquakes have been measured and recorded to be used in future mitigation studies. However in areas of moderate seismicity, such as the mid-America region, high intensity earthquakes are infrequent, and the number of recorded ground motions is inadequate for the development of fragility curves. Many researchers (Hudson 1972; Borcherdt and Glassmoyer 1992; Di

Giulio et al. 2005, etc.) have studied the regional variation of strong ground motions. Local geological conditions have been shown to have a significant impact on strong motion variations and therefore only data from a local region should be used for seismic analyses representing the regional conditions. When there is insufficient recorded data for earthquake records in a region, researchers develop synthetic ground motions. Simulated ground motion records should be representative to a particular area since different soil classifications greatly alter amplifications of different period waves.

Wen and Wu (2001) developed a method to generate ground motion records for three cities in the mid-America region: Memphis, Tennessee, St. Louis, Missouri, and Carbondale, Illinois. Because MAE Center researchers have used these ground motion records for numerous studies (e.g. Wen et al. 2004; Padgett and DesRoches 2006; Jeong and Elnashai 2004), for uniformity these records will also be used in this study. Although uniform hazard response spectra can be used for linear systems, specific ground motion records are needed for a nonlinear analysis. More than one ground motion should be used for a nonlinear analysis due to the large variability of ground motion responses. Multiple simulated records were developed to obtain uniform hazard response spectra for different exceedance probabilities. For ground records from Memphis, TN, Wen and Wu (2001) showed the median value of structural responses under ten suite of records have a very small uncertainty from record-to-record variation when compared to using large number of samples. Therefore only ten ground motions were selected from the multiple developed simulations for each city to most accurately match the uniform hazard response spectra at two different exceedance probabilities, 2% and 10% in 50 years hazard level with the 1997 USGS national earthquake hazard maps (Frankel 2002). The ten records are representative of future earthquakes of various magnitudes, distances, and attenuations, but each simulated record matches the response spectra of a given probability for a wide range of periods. Although ground motion records from other researchers can be applied to this methodology, the twenty representative soil ground motions developed by Wen and Wu (2001) for Memphis, Tennessee are used in this study as shown in Figure 2.1 and Figure 2.2.
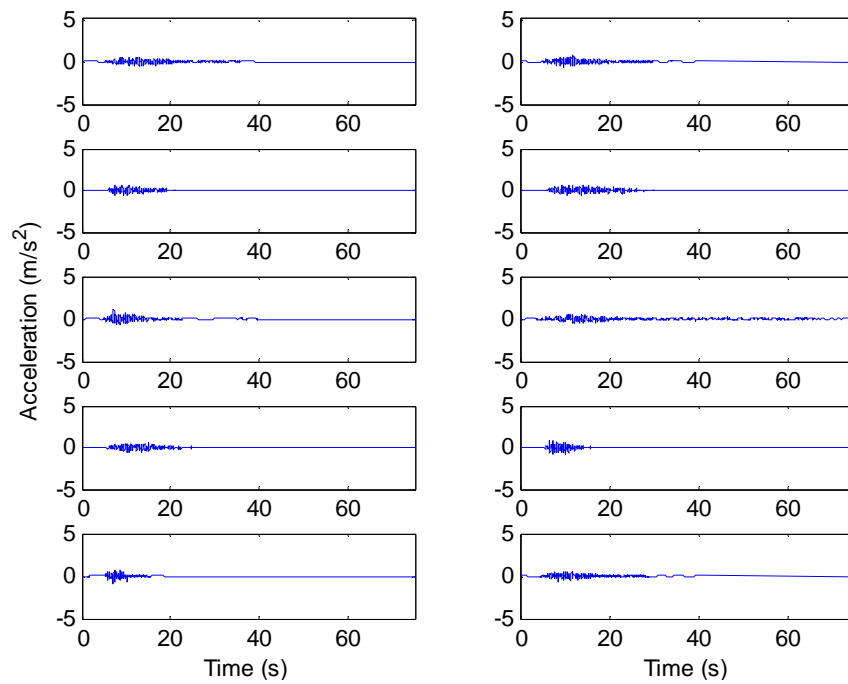
Figure 2.1 Wen and Wu (2001) 10% in 50 Year Ground Motions for Memphis, TN with representative soil
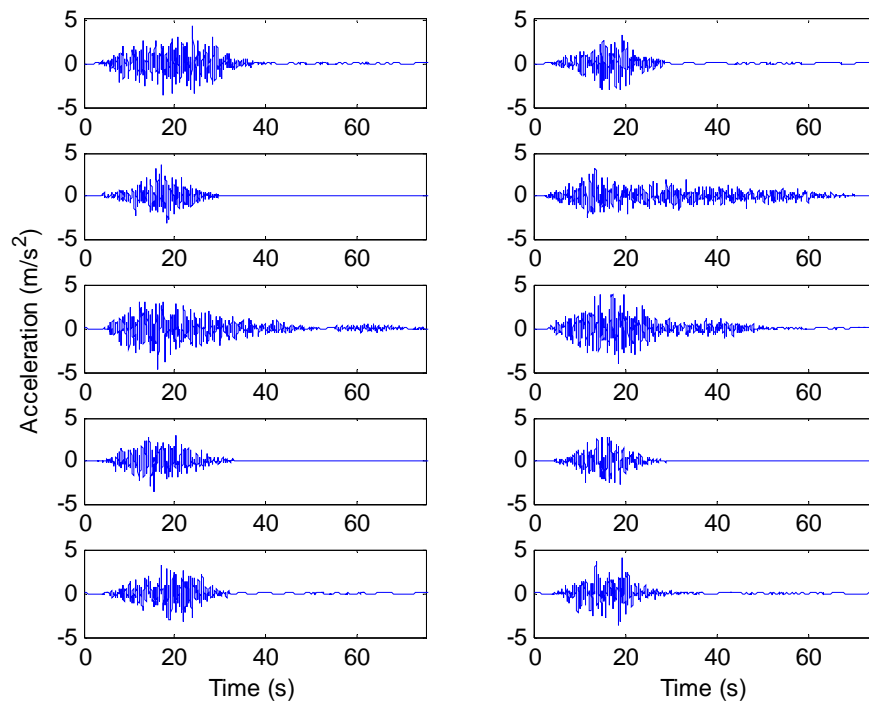
Figure 2.2 Wen and Wu (2001) 2% in 50 Year Ground Motions for Memphis, TN with representative soil

2.1.2 Limit States

A limit state is a criterion defined as the structural demand value where a system is unable to perform at a specified level. Both qualitative and quantitative approaches can be used to classify performance levels. Qualitative approaches are commonly used in the engineering community. FEMA 356: Prestandard and Commentary for the Seismic Rehabilitation of Buildings outlines various qualitative performance levels for structures (FEMA 2000). FEMA 356 is the result of a joint effort between ASCE and FEMA to upgrade the guidelines for seismic rehabilitation of buildings into a national consensus standard. FEMA 356 presents three main structural performance levels to approximate limiting levels of structural damage: immediate occupancy (IO), life safety (LS), and collapse prevention (CP). The post-earthquake damage state of a structure should remain safe to occupy and essentially retain the pre-earthquake design strength to be compliant with the acceptance criteria for the IO structural level. For LS performance level, damage to the structure could occur as long as the structure retains a margin against onset of partial or total collapse. The CP performance level indicates a structure could be on the verge of partial or total collapse, but the structure is still able to support gravity loads. Life safety is often chosen as the desired performance level dictated by minimum design code requirements. FEMA 356 states a maximum interstory drift for different structure types for each performance level. Although interstory drifts are a good estimate of performance levels, researchers should be aware of the uncertainty with a set limit state (Wen et al. 2003).

To date, design codes have only focused on qualitative performance levels. Researchers or designers must perform an analysis of the overall structure to verify member and global values to correspond with quantitative levels. Interstory drift limits from a nonlinear pushover analysis are often used to define First Yield (FY), Plastic Mechanism Initiation (PMI), and Strength Degradation (SD). First yield is the point at which a member starts to yield with an induced lateral loading. When a story mechanism, an overall beam sidesway mechanism, or a hybrid mechanism is created, PMI performance

level has been reached. Strength degradation occurs when the story strength has been degraded by no more than a given percentage of the maximum strength (Wen et al. 2003). An engineer may use these quantitative member and/or global levels to be representative of qualitative levels.

2.1.3   Probability Equation

Moderate to severe earthquakes often cause structures to behave nonlinearly. For a realistic model of a system, the nonlinear behavior must be included in a fragility assessment. Dynamic time history analyses using representative ground motions are analyzed to determine a relationship between structural response demand (D) and earthquake intensity (S). A nonlinear regression analysis is performed assuming a power-law form between the seismic intensity measure and the structural response demand

$$D = aS^b \tag{2.2}$$

where a and b are the unknown constants determined by a logarithmic transformation of Equation (2.2) to a linear form

$$\ln(D) = \ln(a) + b\ln(S) \tag{2.3}$$

Now the constants a and b can be found using a simple linear regression analysis to find the relationship between the structural response demand and the earthquake intensity. When the limit state capacity is defined as a deterministic response limit from code requirements, the fragility can be calculated as

$$F_R = P(D \geq d_0 \mid S = s) = 1 - \Phi\left(\frac{\ln d_0 - \lambda_{D|S}}{\beta_T}\right) \tag{2.4}$$

where d_0 is the limit state capacity, $\lambda_{D|S}$ and β_T are parameters of the lognormal distribution determined from the average value of the best fit power law equation, and β_T is the total uncertainty (Wen et al. 2004). Uncertainty of the building model, the power law equation, and the capacity should all be included in the final result.

For this study, the uncertainty is quantified in three terms: the demand uncertainty ($\beta_{D|S_a}$), the capacity uncertainty (β_{CL}), and the modeling uncertainty (β_M). Further discussion on the effect of uncertainty is discussed in Chapter 4.

2.2 Software Selection

Structures often behave nonlinearly during earthquakes. Thus, analytical models should accurately account for possible nonlinear behavior when simulations are evaluated. Currently, there are no commercial structural analysis programs that directly perform time history analyses for actively or semiactively controlled structures. Thus the challenge arises in choosing appropriate software to facilitate consideration of both a nonlinear model of the structure and the control devices. A control device can easily be modeled in MATLAB (MATLAB 1997). Zeus – Nonlinear (ZeusNL) is a newly developed software program by the MAE Center for inelastic analysis of a structure. ZeusNL can be implemented within the NEES Consortium, a national collaboratory for earthquake engineering, as a computational module (Elnashai et al. 2002). UI-SIMCOR was also developed to coordinate simulations linking various software packages, and is used here to provide an interface between ZeusNL and MATLAB (Kwon et al. 2005). The use of UI-SIMCOR allows the stiffness of the structure to be modeled in ZeusNL while the control device is modeled in MATLAB. The mass of the structure is defined in UI-SIMCOR to calculate the appropriate inertial forces from ground excitation. The target displacements resulting from the sum of the inertial forces and the control forces are used within ZeusNL to calculate the actual displacements of the nonlinear model.

By using UI-SIMCOR, time history responses can be obtained using a nonlinear model of the building with control.

2.2.1   ZeusNL

ZeusNL was developed by MAE Center researchers to provide a completely visual approach to dynamic analyses by featuring a completely visual interface. ZeusNL is able to perform six different types of analysis: nonlinear dynamic and static time-history, conventional and adaptive pushover, eigenvalue and static with non-variable loading. Geometric and material nonlinear behavior is accounted for in both static and dynamic loading. ZeusNL is also able to model the spread of inelasticity along member length and across section depth (Elnashai et al. 2002). Another feature of ZeusNL is the ability to define constant or variable forces, displacements, and accelerations as applied loading, and can vary proportionally or independently in the pseudo-time or time domain (Elnashai et al. 2002). This feature allows ZeusNL to be integrated within the NEES Consortium.

2.2.2   UI-SIMCOR

UI-SIMCOR (University of Illinois -- Simulation Coordinator) is a distributed-hybrid simulation platform. It was originally developed to remotely link static analysis and experimental modules together in the NEES Consortium (Kwon et al. 2005). The remote sub-structured pseudo-dynamic test is performed by a time step integration scheme. The alpha operator splitter (α-OS) method determines the next new set of displacements to apply to each static or experimental module for a given input ground motion time step. The α-OS method is often used for pseudodyamic testing because this non-iterative implicit time integration scheme provides unconditional numerical stability (Shing and Vannan 1991). The communication between software programs occurs over a Network Telepresence Control Protocol (NTCP) server or a Transmission Control Protocol/Internet Protocol (TCP/IP) network. UI-SIMCOR

facilitates communication between programs and ZeusNL communicates using NEES Sam, which is an intermediary interface.

Six steps are performed to create a computational simulation using these tools. First, the decision of how to sub-structure the desired experiment is made. In this study, ZeusNL is used to model the stiffness of the structure and MATLAB is used to model the control devices. Second, the effective degrees of freedom and the location of lumped masses for each module are defined. The static model, ZeusNL herein, is then created to be compatible with UI-SIMCOR. Network ports are then opened and communication is configured in the necessary module files. Next, MATLAB files within UI-SIMCOR are modified to define the particular experiment. After NEES Sam is opened, UI-SIMCOR can be loaded to begin the simulation.

UI-SIMCOR simulates the pseudodynamic test by first finding the initial stiffness matrix of the structure using the direct stiffness method. Figure 2.3 shows the flowchart of the iterative process to perform a pseudodynamic test using UI-SIMCOR and ZeusNL. The target displacement and velocity are found using the α-OS method, which is a modified Newton iteration that is unconditionally stable (Shing and Vannan 1991). This integration method was selected to be used within UI-SIMCOR because the software was designed for pseudodynamic tests to minimize experimental errors. The force from the control devices are also determined and added to the structure's inertial forces. Force loads at the effective degrees of freedom are then communicated through NEES Sam to determine the structure's restoring force.
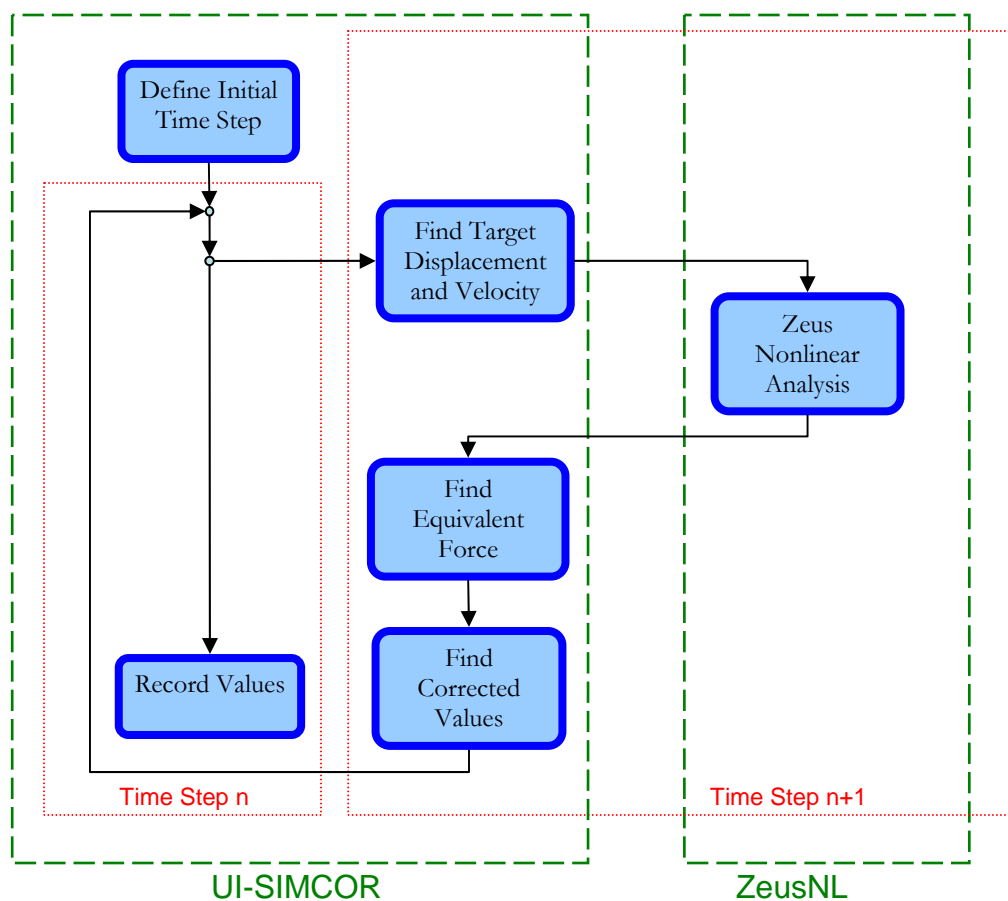
Figure 2.3 Flow Chart of UI-SIMCOR Simulation

2.2.3 Verification of Software Selection

To verify the accuracy of the models within UI-SIMCOR, a time history responses from a ground motion record was performed to compare results using UI-SIMCOR to results obtained from a linear dynamic time history analysis using the Newmark integration scheme in ZeusNL. The same ground motion record and time step (0.005 sec) was defined in each analysis. Because UI-SIMCOR and ZeusNL model damping differently, zero damping was defined in both analyses for this verification. **Error! Reference source not found.** shows the interstory displacement responses of the three story steel moment frame structure to be described in Chapter 3.
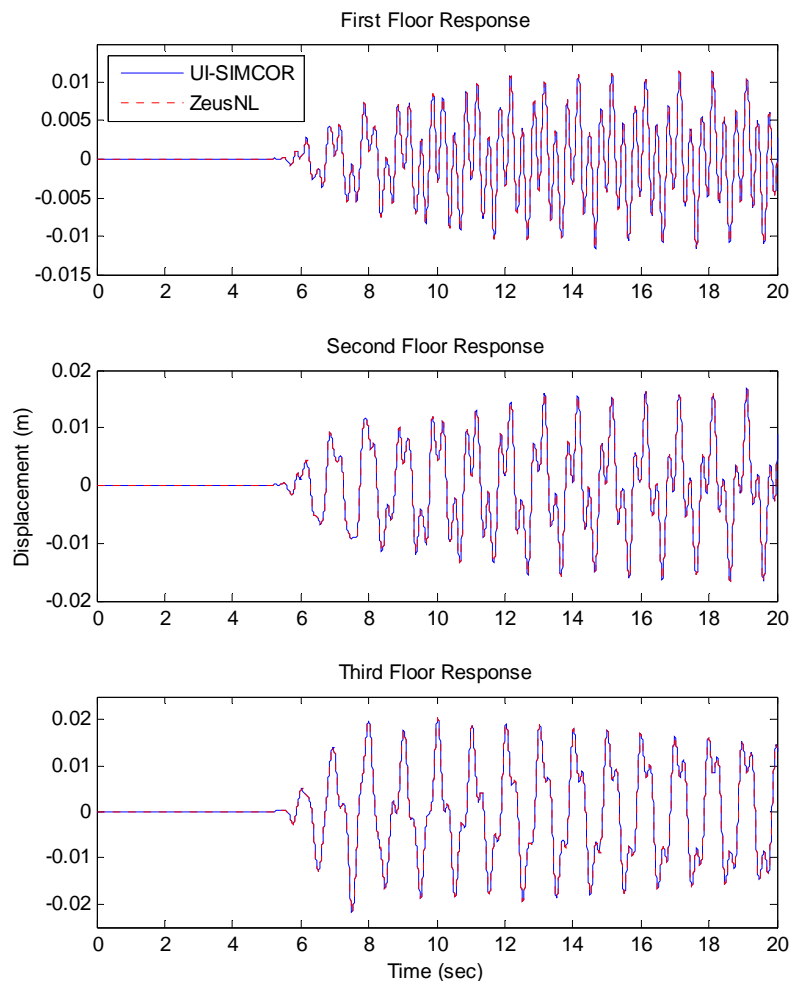
Figure 2.4 Comparison of Responses of UI-SIMCOR Results with ZeusNL Results

The distinction between the two methods is very difficult to detect in Figure 2.4 because negligible errors (less than 0.5%) exist in the interstory drifts when using UI-SIMCOR with ZeusNL compared to using the dynamic analysis in ZeusNL. This verification confirms that UI-SIMCOR is a reliable simulation coordinator for the required analyses.

2.3   Structural Control

Structural control is an effective means to minimize structural responses during dynamic loads. This thesis focuses on the fragility of passive and active systems. The following

section discusses the modeling of those systems and devices, as well as an optimal device placement strategy.

2.3.1 Passive and Active Control: Modeling and Algorithm Development

A controlled structural system with feedback control can be represented as a block diagram in Figure 2.5. The inputs to the structural system are the disturbance ($\mathbf{w}$) and control force vector ($\mathbf{u}$) and the outputs are the measured output vector ($\mathbf{y}$) and the regulated output vector ($\mathbf{z}$). The disturbance to the system for this study is ground excitation. The regulated output may contain any linear combination of the states of the system and the control input.
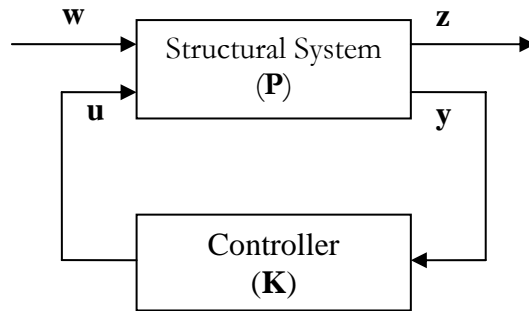
Figure 2.5 Block Diagram of Controlled Structural System

Assuming that the forces provided by the control devices are adequate to keep the response of the structure within the linear region and the only disturbance ($\mathbf{w}$) to the system is ground excitation ($\ddot{x}_g$), the equations of motion of the structural system can be written in the following state-space form

$$\dot{\mathbf{x}}_s = \mathbf{A}\mathbf{x}_s + \mathbf{B}\mathbf{u} + \mathbf{E}\ddot{x}_g$$
$$\mathbf{y} = \mathbf{C_y}\mathbf{x}_s + \mathbf{D_y}\mathbf{u} + \mathbf{F_y}\ddot{x}_g + \mathbf{v} \qquad (2.5)$$
$$\mathbf{z} = \mathbf{C_z}\mathbf{x}_s + \mathbf{D_z}\mathbf{u} + \mathbf{F_z}\ddot{x}_g$$

where $\mathbf{x}_s$ is the state vector, $\ddot{x}_g$ is a one-dimensional ground acceleration, $\mathbf{u} = [f_1, f_2, ... f_n]'$ is the vector of n measured control forces, $\mathbf{y}$ is the vector of measured outputs, $\mathbf{v}$ is the measurement noise vector, and $\mathbf{z}$ is the regulated output vector (Yi and Dyke 2000).

The control devices in this study are modeled as ideal devices. Thus actuator dynamics and control-structure interaction are not included in the device models. The passive devices used in this study are assumed to be ideal viscous dampers, with a force of

$$f_i(t) = -c_i \dot{x}_{di}(t)$$

(2.6)

where $\dot{x}_{di}$ is the relative velocity across the ith device and c_i is the damping coefficient associated with the ith device. A range of values are considered to vary the force capacity of the device.

Accelerometers are a practical, inexpensive and readily available way to measure a structure's responses. Thus, absolute accelerations of the floors of the structures are typically used in feedback control (Dyke et al. 1996b). Therefore, measurements typically available for active control force determination include the absolute acceleration of selected points on the structure, the displacement of each control device, and a measurement of each control force. The active devices used in this study are modeled as ideal force actuators. Ideal actuators are assumed to have the ability to instantaneously and precisely supply the force commanded by the control algorithm. Thus, the force provided by the active control device is given by

$$f_i(t) = u_i$$

(2.7)

where $u_i(t)$ is the ith command force determined with the control algorithm. Notice that no actuator dynamics or control-structure interaction are considered in this ideal model although these will have significant effects in a physical system (Dyke 1995).

An H_2/LQG control law has been shown to be effective for seismically excited structures (Dyke et. al. 1995, 1996a, 1998; Jansen and Dyke 2000) even in the case of nonlinear behavior (Yoshida and Dyke 2004). H_2 control minimizes the RMS response of the structure due to a broad-band excitation. The first mode response will be reduced greater than higher modes because the first mode is the largest contributor to the RMS response and will be primarily modified to reduce the RMS response (Spencer et al. 1994). In this approach $\ddot{x}_g$ is taken to be a stationary white noise, and an infinite horizon performance index is chosen that weights the regulated output vector, $\mathbf{z}$, i.e.,

$$J = \lim_{\tau \to \infty} \frac{1}{\tau} \mathrm{E}\left[\int_0^\tau \left\{ (\mathbf{C}_z\mathbf{x} + \mathbf{D}_z\mathbf{u}_c)'\mathbf{Q}(\mathbf{C}_z\mathbf{x} + \mathbf{D}_z\mathbf{u}_c) + \mathbf{u}_c'\mathbf{R}\mathbf{u}_c \right\} dt \right] \tag{2.8}$$

where $\mathbf{R} = \mathbf{I}$, and the elements of the weighting matrix $\mathbf{Q}$ are selected to appropriately weight the regulated outputs. Further, the measurement noise is assumed to be identically distributed, statistically independent Gaussian white noise processes, and $S_{\ddot{x}_g \ddot{x}_g} / S_{v_i v_i} = \gamma = 25$. The control law is of the form

$$\mathbf{u}_c = -\mathbf{K}\hat{\mathbf{x}} \tag{2.9}$$

where $\hat{\mathbf{x}}$ is the Kalman filter estimate of the state vector. The matrix $\mathbf{K}$ is the full state feedback gain matrix for the deterministic regulator problem. The measured output vector containing the accelerations is not a full state vector and the Kalman filter estimator for the states of the system are given by

$$\dot{\hat{\mathbf{x}}} = \mathbf{A}\hat{\mathbf{x}} + \mathbf{B}\mathbf{u}_c + \mathbf{L}(\mathbf{y} - \mathbf{C}_y\hat{\mathbf{x}} - \mathbf{D}_y\mathbf{u}_c)$$
$$\mathbf{L} = \mathbf{R}^{-1}\left(\gamma \mathbf{F}_y\mathbf{E}' + \mathbf{C}_y\mathbf{S} \right) \tag{2.10}$$

where **R**, **S**, and **E** are the parameter matrices with appropriate dimension described in more detail in Spencer et al. 1998. In the active control designs, various weighting cases are examined to determine the best strategy for controlling the structure. Furthermore, to compare control devices with a range of force capacities, the weightings on the regulated outputs are varied. Thus, active and passive devices with like force capacities can be compared directly.

2.3.2   Optimal Placement

One additional design consideration is cost for controlled systems. A designer would like to minimize the number of devices placed in a structure while still reducing the responses. For simple systems, experienced engineers are able to use engineering judgment to determine device and sensor placements. For more complex systems, optimal placement is a solution to randomly selecting placements. Optimal placement is used in this study to determine the control device locations and a sensor is assumed to be placed at every story for active control. This optimal placement technique can also be applied to sensor placement if it is desirable to reduce the number of sensors.

Gawronski (1998) proposes determining the norm of each device for selected modes and grading each device according to their participation in the whole system norm. If given a large set of device placements, the optimal placement problem involves determining the locations of a smaller subset of placements such that the H_2, H_∞, or Hankel norms of the subset is as close as possible to the norm of the original set (Gawronski 1998). However, Hankel norms are an appropriate measure for placement since Hankel singular values do not vary with coordinate transformations (Wang 2006). This approach discussed in detail in Wang (2006) is briefly described below.

If the state-space representation $(\mathbf{A}_m, \mathbf{B}_m, \mathbf{C}_m)$ of a building model is considered, the Hankel norm of the ith mode is determined by

$$\left\|G_i\right\|_h = \gamma_i \cong \frac{\left\|\mathbf{B}_{mi}\right\|_2 \left\|\mathbf{C}_{mi}\right\|_2}{4\zeta_i \omega_i} \qquad (2.11)$$

where $\left\|\cdot\right\|$ denotes the Hankel norm. The Hankel norm is approximately equal to half of the H_∞ norm. The relationship between the Hankel norm of a structure with a single device and the Hankel norm of a set of devices is that the Hankel norm with a set of devices is the RMS sum of the Hankel norm with each single actuator from this set

$$\gamma_i = \sqrt{\sum_{j=1}^{s} \gamma_{ij}^2} \qquad (2.12)$$

Then, the Hankel norm of the system is the largest norm of its mode

$$\left\|G\right\|_h \cong \max_i \left\|G_i\right\|_j = \gamma_{max} = 0.5\left\|G\right\|_\infty \qquad (2.13)$$

where γ_{max} is the largest Hankel singular value of the system. The device index σ_{ij} that evaluates the jth device at the ith mode in terms of the Hankel norm is

$$\sigma_{ij} = \frac{\left\|G_{ij}\right\|_h}{\left\|G\right\|_h} \qquad (2.14)$$

where each column can be looked at individually to determine the effect of each device to a single mode and each row can be studied to determine the overall effect of a single device to all modes of the structure. A higher performance index indicates the location of the device would be more beneficial than at a location with a lower index value. If certain modes of a structure are of particular interest, this method allows one to find an optimal location for a particular mode. However, when multiple devices are often placed in structures, highly correlated locations should be considered to optimize the placement configuration. To determine whether device locations are correlated, a vector of the squares of the ith Hankel modal norms is defined

$$g_i = \begin{bmatrix} \left\|G_{i1}\right\|_h^2 \\ \left\|G_{i2}\right\|_h^2 \\ \vdots \\ \left\|G_{in}\right\|_h^2 \end{bmatrix} \tag{2.15}$$

The correlation coefficient of the kth mode at the ith control device location is equated as

$$\rho_{ik} = \frac{g_i^T g_k}{\left\|g_i\right\|_2 \left\|g_k\right\|_2}, i = 1, \ldots, r, k = i+1, \cdots, r. \tag{2.16}$$

The correlation coefficient is used to determine which locations are highly correlated and when considering the higher performance indices, the optimal placement configuration can be found (Wang 2006).

2.4 Summary

The five main steps to develop a fragility relationship are outlined in this chapter. Discussion includes appropriate ground motion records, prescribed limit states, and the probability equation. Appropriate software is chosen to evaluate a nonlinear time history analysis with a control device. UI-SIMCOR is the chosen simulation coordinator that communicates between ZeusNL which models the nonlinear stiffness of the structure and MATLAB which models the mass and determines the control and inertial forces from earthquake excitations. The algorithm development of the passive and active systems is presented along with an optimal device placement technique.

Chapter 3

3-Story Building Model and Uncontrolled Fragility

This chapter describes the building model used for demonstrating the method of developing fragility curves for structures with control devices. The building is a 3-story steel moment frame structure typical of a seismic region. The fragility curve of the uncontrolled structure is also presented.

3.1   Description of Building

A typical low-rise building that meets seismic codes was chosen for demonstration of the procedure to develop a fragility curve for a controlled structure. The building model used for this study is based upon the 3-story benchmark building described in Ohtori et al. (2004). The steel moment-resisting frame structure is one of three nonlinear benchmark structures designed for the Los Angeles, California area by Brandow & Johnston Associates for the SAC Phase II Steel Project (SAC Steel Project 1994). The SAC Steel Project was a joint venture of Structural Engineers Association of California (SEAOC), Applied Technology Council (ATC), and California Universities for Research in Earthquake Engineering (CUREE) funded by the Federal Emergency Management Agency (FEMA) to study the brittle behavior of welded steel frame structures. This building was chosen for this study because it is a typical low-rise steel structure designed for an earthquake prone region and has been studied by multiple researchers.

The structure is 36.58m by 54.97m in plan, and 11.89m in elevation. There are six 9.15m bays in the strong (east-west) direction and four 9.15m bays in the weak (north-south) direction. Floor-to-floor heights are 3.96m. All measurements are to the center line of the elements. Steel perimeter moment-resisting frames are used for the lateral load-resisting system as seen in Figure 3. where the triangles represent a moment connection. A 2-D model of the weak (north-south) direction of the building is used for the analysis. The columns are 345MPa steel wide flanges and the beams are 248MPa steel wide flanges. The size of each component of the 2-D frame is shown in Figure 3.1.
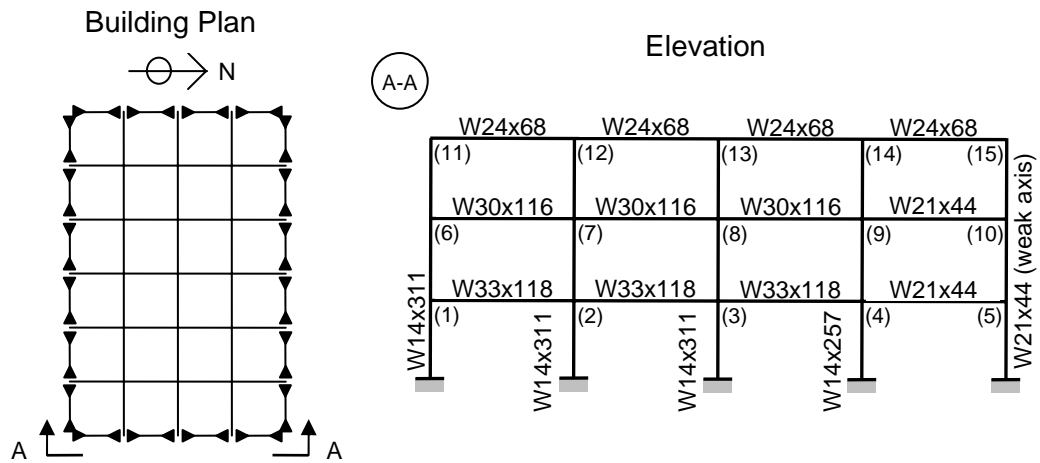
Figure 3.1 Building Plan and Elevation View of Building Model

The first and second levels both have 9.57×10^5kg and the third level has 1.04×10^6kg of seismic mass for both N-S moment resisting frames. Since the inertial forces consist of the seismic mass of the floor slab, ceiling, flooring, mechanical, electrical, and roofing, the seismic mass of each story is lumped into five nodes with respect to area. The locations of the fifteen nodes are shown in Figure 3.1.

3.2   Analytical Model

ZeusNL is used to analytically model the stiffness of the structure. The building consists of two different materials: 248MPa steel for the beams and 345MPa steel for the columns. A bilinear elasto-plastic model with kinematic strain-hardening is used for both materials. The material properties used to model each material are shown in Figure 3.2 and defined in Table 3.1.

Table 3.1 Material Properties

Property	Description	Beam Properties	Column Properties
E	Young's Modulus	200,000 N/m^2	200,000 N/m^2
σ_y	Yield Strength	248 MPa	345 MPa
μ	Strain-hardening Parameter	0.05	0.05

Figure 3.2 Bilinear Elasto-plastic Model after Elnashai et al. 2002

Each W-shape member shown in Figure 3.1 is defined in ZeusNL using dimensions from the Manual of Steel Construction (AISC 2001). Each member is divided into four elements for accurate inelastic modeling. Each element is defined as a cubic elasto-

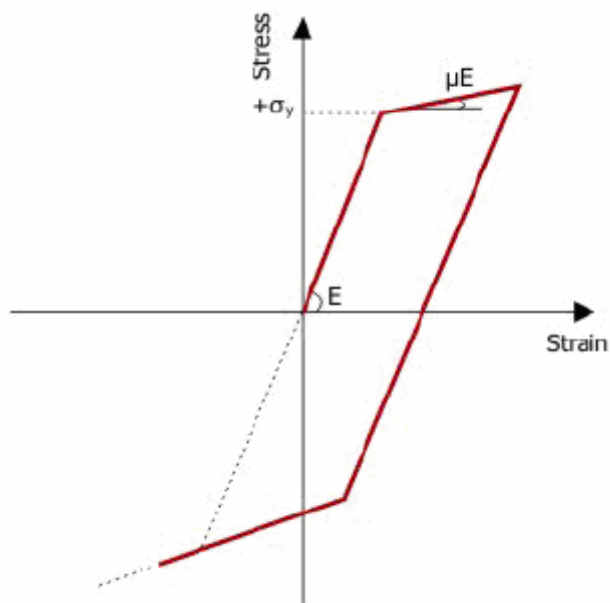plastic 3D beam-column element to model the spread of inelasticity along the member length and across the section depth, by dividing the cross-section at the two Gauss points in 200 monitoring areas (Elnashai et at. 2002). Structural nodes, represented by blue squares, are defined to connect each element, represented by black lines in Figure 3.3. Each structural node is restrained out-of-plane and the ground level nodes are fully fixed.
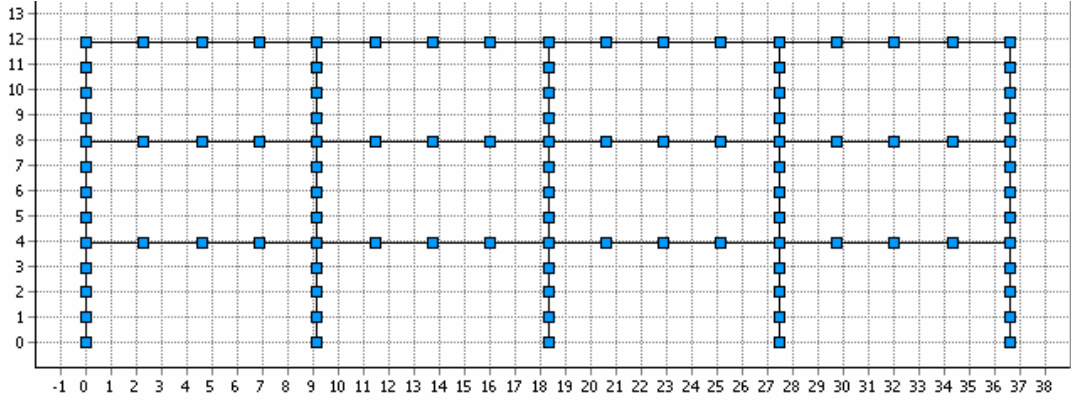
Figure 3.3 ZeusNL Model

When using UI-SIMCOR, the mass of the structure is defined within MATLAB. The seismic mass at each story is divided into five nodes with respect to area such that the outermost nodes have half the mass as the interior nodes.

The assumption of Raleigh damping is used to form the modal damping matrix **C**, defined as

$$\mathbf{C} = c_1 \cdot \mathbf{T}_R^T \mathbf{M} \mathbf{T}_R + c_2 \cdot \mathbf{T}_R^T \mathbf{K} \mathbf{T}_R \tag{3.1}$$

where c_1 and c_2 are chosen such that the modal damping ratios are $\zeta_1 = \zeta_2 = 0.02$, $\mathbf{T}_R$ is the transformation matrix, **M** is the mass matrix, and **K** is the stiffness matrix. According to Raleigh damping, the damping in the third mode is found by:

$$\zeta_i = \zeta_1 \left(\omega_1 \omega_2 + \omega_i^2 \right) / \left(\omega_i \omega_1 + \omega_2^2 \right) \tag{3.2}$$

where ω_i is the ith natural frequency. The damping of the third mode is found to be $\zeta_3 = 0.0296$.

3.3   Validation of the Model

To ensure the building model in ZeusNL is an accurate analytical representation of the structure, the results of an analysis was compared to the benchmark structure. An eigenvalue analysis within ZeusNL was performed to find the first three modes of the structure. For an eigenvalue analysis in ZeusNL, lumped (concentrated) mass elements are used to model the seismic mass. The seismic mass is distributed with respect to area similar to UI-SIMCOR. Table 3.2 shows the first three natural frequencies of both the ZeusNL model and the results found by Ohtori et al. (2004).

Table 3.2 Comparison of Natural Frequencies

	Zeus-NL Model	Benchmark Structure
Mode 1	1.00 Hz	0.99 Hz
Mode 2	3.03 Hz	3.06 Hz
Mode 3	5.41 Hz	5.83 Hz

The eigenvalues from the ZeusNL model are slightly different from the values reported in the benchmark paper. Slight differences in the models could account for the difference. The benchmark structure assumed three of the connections were not fully fixed and the beams were modeled as rigid. However, the ZeusNL model assumed all connections were moment-resisting connections and the beams were not modeled as infinitely stiff. Because the first mode has only 1% error between the two models, the ZeusNL model is assumed to be an accurate representation of the structure.

3.4 Fragility Curves of the Original Structure

To compare the performance of the controlled to the uncontrolled structure, a fragility curve of the original uncontrolled structure is found. The five main steps described in Chapter 2 are performed. The ground motion records chosen for this study are the synthetic ground motions developed by Wen and Wu (2001) for Memphis, TN with representative soil. The seismic demands (or intensity measures) are found for each earthquake. Two demands are used in this study: peak ground acceleration (PGA) and spectral acceleration (S_a). While PGA is the maximum acceleration of the earthquake record, spectral acceleration is the maximum acceleration response of a harmonic oscillator with the same natural frequency as the structure. Spectral acceleration has been widely used as an intensity measure for analysis of structural responses of a single frame (Baker and Cornell 2006). A single degree of freedom system with frequency of 1.00Hz and a damping of 2% is used to calculate S_a. From Figure 3.4, the higher intensity earthquakes with a probability of 2% in 50 years are labeled as numbers one through ten and the 10% in 50 year earthquakes are labeled as numbers eleven through twenty.
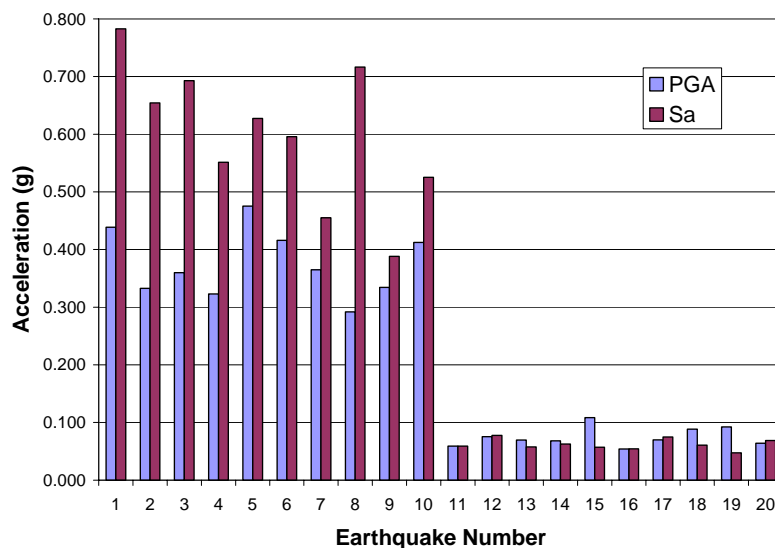
Figure 3.4 Seismic Intensities of Wen and Wu Simulated Ground Motion Records

The second step to develop a fragility relationship is to develop an analytical model of the structure, which is described in Section 3.2. The stiffness is modeled in ZeusNL, and the mass and damping are defined within UI-SIMCOR. Since there is no control system on the original structure, no control force is defined within the analytical model.

The nonlinear time history analyses for the twenty earthquake records are computed. The maximum transient interstory drifts at each story level are shown in Figure 3.5. The maximum interstory drift for each ground motion record occurs at the top story, which can be explained by the facts of the building has more seismic mass at the top story and the building does not have a soft story since all story heights are the same. The permanent drifts from the nonlinear analysis are shown in Figure 3.6. The range of permanent drift values from the same hazard occurrence level demonstrates the importance of using more than one earthquake record for a nonlinear analysis.
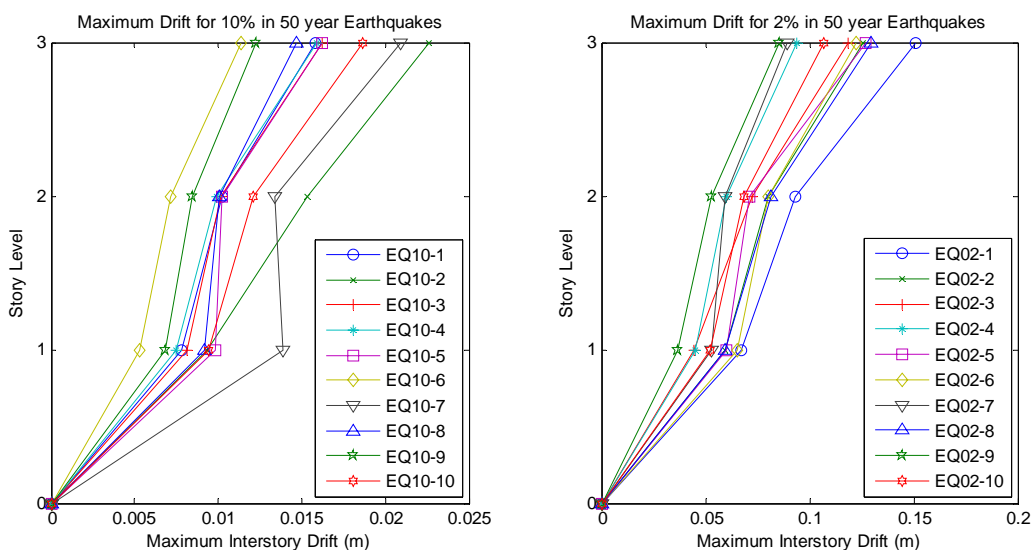
Figure 3.5 Maximum Interstory Drift of Original Structure for Each Ground Motion Record
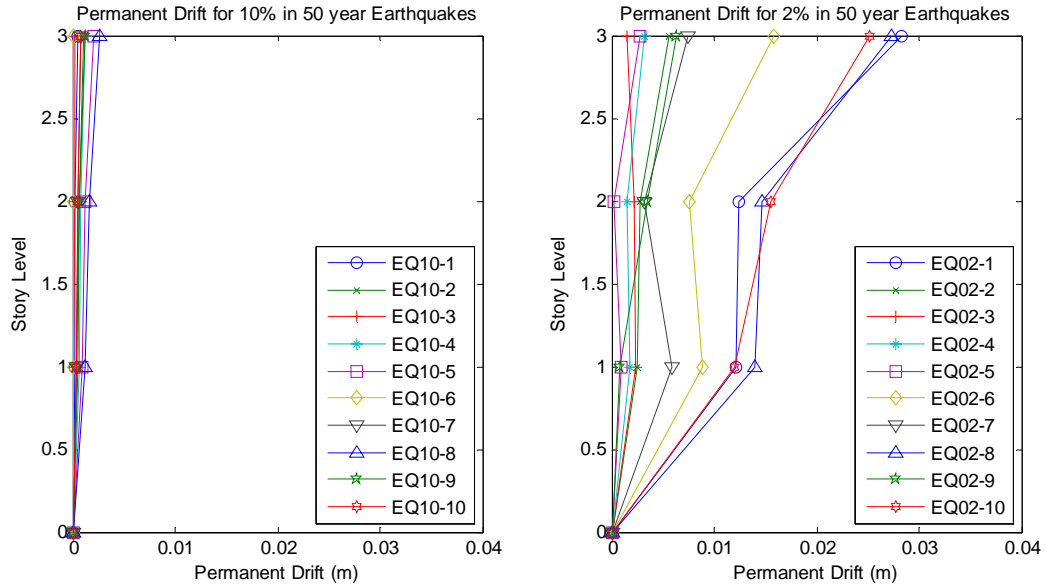
Figure 3.6 Permanent Drifts of Original Structure for Each Ground Motion Record

To calculate a probabilistic seismic demand model, the maximum drift of each record is plotted against the record's demand to calculate a regression analysis between the seismic intensity measure and the structural response demand. A nonlinear regression analysis of the power-law form is used due to the nonlinear nature of the problem. Using a logarithmic transformation of the power law equation as described in Chapter 2, a linear regression analysis determines the unknown constants. The two best fit power law equations from Figure 3.7 are determined as

$$Y_{P_{S_a}} = 4.5451 S_a^{0.8653}$$
$$R^2 = 0.9924$$

(3.3)

$$Y_{P_{PGA}} = 8.6515 PGA^{1.155}$$
$$R^2 = 0.9317$$

(3.4)

where Y_p is the power law predicted demand. The R^2 values indicate that spectral acceleration is a better intensity measure than PGA. The demand uncertainty accounts for the uncertainty in the power law equations and is discussed in further detail in

Chapter 4. Figure 3.7 plots each ground motion record as a plus sign and the best fit power law equation as the black line.
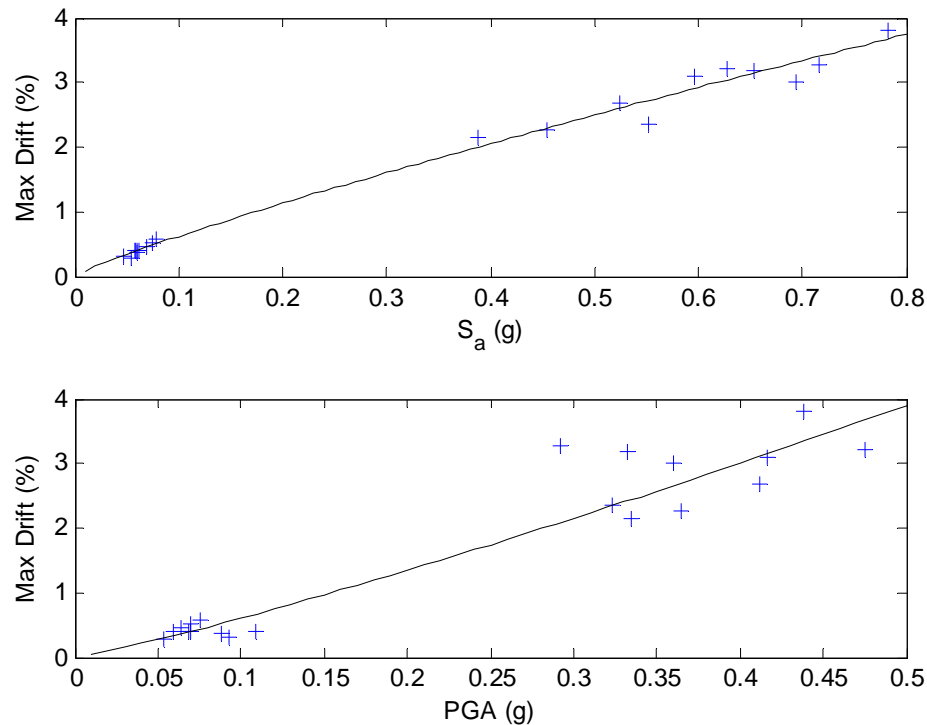
Figure 3.7 Probabilistic Seismic Demand Model for Original Structure

The American Society of Civil Engineers had defined target building performance levels in FEMA 356. These target performance levels are described qualitatively in terms of extent of damage to the building. Three main performance levels are defined: immediate occupancy (IO), life safety (LS), and collapse prevention (CP). Table 3.3 shows the performance levels for vertical elements for steel moment frames. FEMA 356 defines interstory drift values associated with each performance level that are typical values of the overall performance of the structure, but it is noted that some variation in actual performance should be expected due to inherent uncertainties. Note that Table 3.3 is for steel moment frame structures and the acceptable limits for other types of structures may differ. The drift limits defined by FEMA for the three structural

performance levels are used for this study and the uncertainty in the capacity is accounted for within the fragility equation.

Table 3.2 Structural Performance Levels and Damage for Steel Moment Frames (FEMA 356)

	Structural Performance Levels		
Type	Collapse Prevention	Life Safety	Immediate Occupancy
Primary	Extensive distortion of beams and column panels. Many fractures at moment connections, but shear connections remain intact.	Hinges form. Local buckling of some beam elements. Severe joint distortion; isolated moment connection fractures, but shear connections remain intact. A few elements may experience partial fracture.	Minor local yielding at a few places. No fractures. Minor buckling or observable permanent distortion of members.
Secondary	Same as primary.	Extensive distortion of beams and column panels. Many fractures at moment connections, but shear connections remain intact.	Same as primary.
Drift	5% transient or permanent	2.5% transient; 1% permanent	0.7% transient; negligible permanent

Wen et al. (2004) provided the equation used to develop the fragility relationship

$$P(LS \mid S_a) = 1 - \Phi\left(\frac{\lambda_{CL} - \lambda_{D|S_a}}{\sqrt{\beta_{D|S_a}^2 + \beta_{CL}^2 + \beta_M^2}} \right) \tag{3.5}$$

where Φ is the standard normal distribution, λ_{CL} =ln(median drift capacity for a particular limit state), $\lambda_{D|S_a}$ = ln(calculated median demand drift given the spectral acceleration from the best fit power law line), $\beta_{D|S_a}$ = demand uncertainty = $\sqrt{\ln(1+s^2)}$, where s^2 = standard error = $\sum \left[\ln(Y_i) - \ln(Y_p)\right]^2 / (n-2)$, Y_i and Y_p are the observed and power law predicted median demand drifts, respectively, given the spectral acceleration, and n is the number of sample data demand points, β_{CL} is the capacity uncertainty, and β_M is the modeling uncertainty. The capacity and modeling

uncertainty are taken as 0.3 for this study because this value is often used in other fragility analyses (Wen et al. 2004; Bai 2004). A parameter study on the uncertainty values is presented in Chapter 4.

Using Equation 3.5, a fragility curve is plotted in Figure 3.8 using S_a as the intensity measure for the three different limit states: IO, LS, and CP. Because the slope or shape of the curve is controlled by the uncertainty, the curves show that there is much more uncertainty associated with the collapse prevention limit state as expected. When the intensity measure is S_a=0.5g, the performance level immediate occupancy is almost guaranteed to be exceeded, but there is only about 5% probability of reaching life safety and 0.5% probability of exceeding collapse prevention.
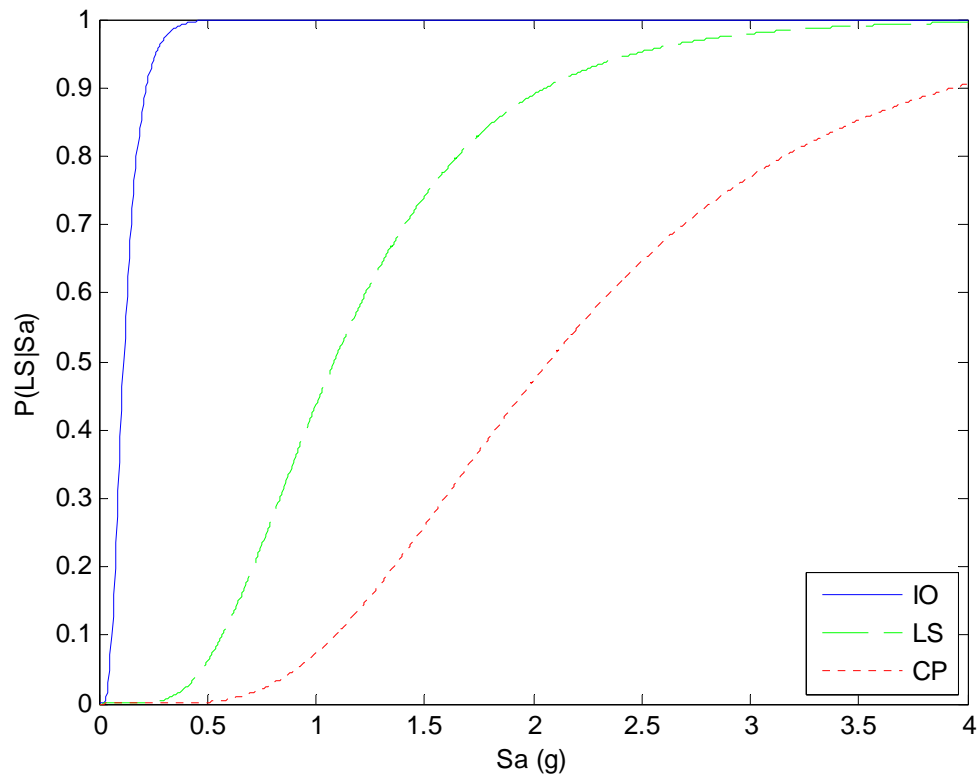
Figure 3.8 Fragility Curve for Original Steel Moment Resisting Frame using S_a

An equation analogous to Equation 3.5 is used when the intensity measure is PGA

$$P(LS \mid PGA) = 1 - \Phi\left(\frac{\lambda_{CL} - \lambda_{D|PGA}}{\sqrt{\beta_{D|PGA}^2 + \beta_{CL}^2 + \beta_M^2}} \right) \tag{3.6}$$

where $\lambda_{D|PGA}$ = ln(calculated median demand drift given the peak ground acceleration from the best fit power law line) and $\beta_{D|PGA}$ = demand uncertainty. Using this equation, the fragility curve for the original building is shown in Figure 3.9 using PGA as the seismic demand. More error is present in the best-fit power law equation when PGA is used as the hazard demand and therefore, the smaller slopes of the fragility curves depict more uncertainty in the system.
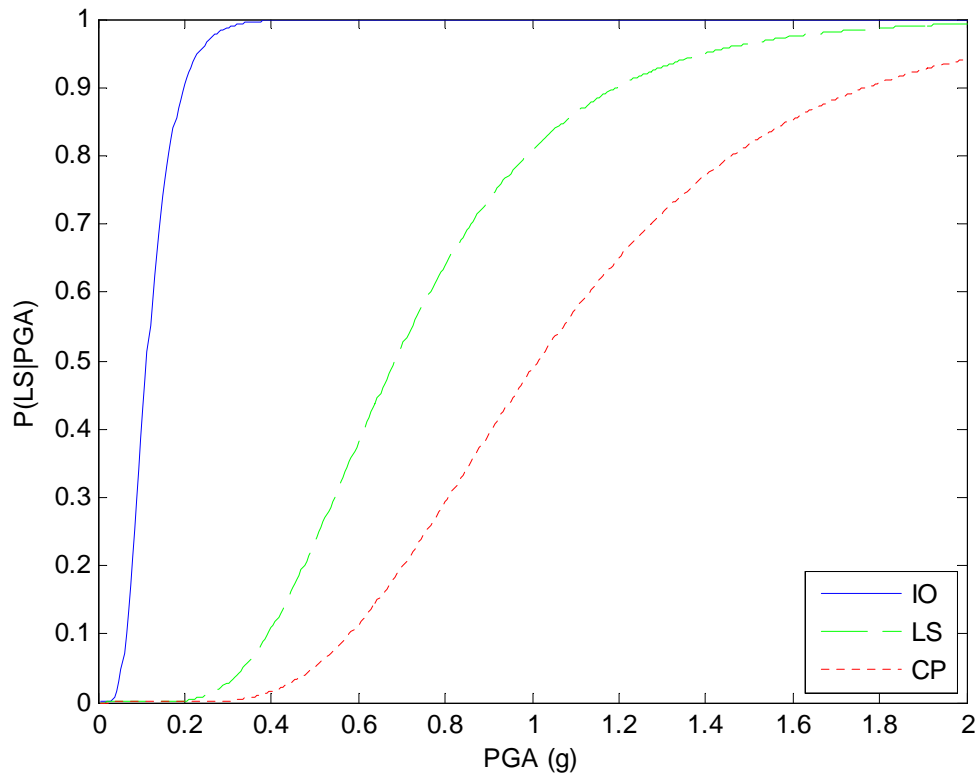
Figure 3.9 Fragility Curve for Original Steel Moment Resisting Frame using PGA

3.5   Summary

This chapter defines the case study structure, a three-story steel moment resisting building with four bays. The North-South moment resisting frame is used in the analysis. A description of the analytical model has is provided in which ZeusNL is used to model the stiffness of the structure and UI-SIMCOR acts as a simulation coordinator to perform the nonlinear time history analyses. The five main steps to develop a fragility curve are demonstrated using the original structure with no retrofit. Ground motion records developed by Wen and Wu from (2001) for Memphis, TN with representative soil are used for the analysis. After calculation of the probabilistic seismic demand model, the fragility curves for the original structure are presented using both S_a and PGA as earthquake demand measures and appropriate equations that explicitly include uncertainty.

Chapter 4

A Parameter Study on the Uncertainty in a Fragility Analysis

This chapter investigates the influence of uncertainty in a fragility analysis. A parameter study on the demand, modeling, and capacity uncertainty is presented, and the values used for these uncertainty parameters are defined.

4.1 Total Uncertainty

One challenge of a seismic risk assessment is defining a systematic way to treat uncertainty and properly accounting for all sources of uncertainty. Wen et al. (2003) wrote a living document for the MAE Center to describe various methods and procedures an earthquake-engineering professional can understand and use to address the issues of uncertainty modeling in earthquake engineering. Two types of uncertainty are present in a fragility analysis: aleatory and epistemic. Aleatory uncertainty is inherently random and irreducible by additional knowledge or data. Construction errors and the variability in material properties are examples of aleatory uncertainty in a fragility analysis. Epistemic uncertainty is due to ignorance. Because epistemic uncertainty is dependent on the model, it is reducible with additional knowledge or data (Wen et al. 2003). Examples of epistemic uncertainty are the differences in analytical programs and the assumed loading distribution to determine the critical response.

MAE Center researchers have categorized the total uncertainty of a fragility analysis into different parameters: the demand uncertainty ($\beta_{D|S_a}$), the capacity uncertainty (β_{CL}), and the modeling uncertainty (β_M). The difference between the power-law predicted

median demand drift and the observed simulated drift is accounted for in the demand uncertainty. Uncertainty in the defined limit states is defined within the capacity uncertainty parameter. Epistemic uncertainty arises from using one set of ground motions over competing models. Uncertainty is also present in the building materials. Material properties are inherently random. Although Ellington et al. (1980) showed that the coefficient of variation of the yielding strength is around 10% or less for steel members, this aleatory uncertainty should be included in the total uncertainty. Uncertainty in the structure and control model is also integrated within the modeling uncertainty parameter.

Three parameters have been identified by MAE Center researchers to quantify uncertainty in a fragility analysis. For the original building model without control, a parameter study is performed to investigate the influence of the uncertainty parameters on the fragility analysis. Uncertainty of the building model, the power law equation, and the capacity are all included in the final result. The total uncertainty of the system is defined as

$$\beta_T = \sqrt{\beta_{D|S_a}^2 + \beta_{CL}^2 + \beta_M^2}$$ (4.1)

where $\beta_{D|S_a}$ is the demand uncertainty, β_{CL} is the capacity uncertainty, and β_M is the modeling uncertainty. These three uncertainty parameters will be investigated in the next sections.

For the following parameter studies, the 3-story steel moment frame building model described in Chapter 3 with no control devices is used. Representative earthquakes from Memphis, TN are chosen as the ground motion records (Wen and Wu 2001). The life safety limit state of 2.5% transient drift is defined.

4.2   Demand Uncertainty

The demand uncertainty ($\beta_{D|S_a}$) is determined from the standard error (s^2) of the power law predicted demand drift equation as

$$\beta_{D|S_a} = \sqrt{\ln(1 + s^2)} \tag{4.2}$$

$$s^2 = \sum \left[\ln(Y_i) - \ln(Y_p)\right]^2 \big/ (n - 2) \tag{4.3}$$

where Y_i and Y_p are the observed and power law predicted median demand drifts, respectively, given the spectral acceleration, and n is the number of sample data demand points. The demand uncertainty is dependent on the best fit equation, the number of earthquake records, and the chosen intensity measure.

The best fit equation is determined by a regression analysis of the intensity measure of the ground motion and the demand measure on the structure. Although other nonlinear equations maybe used if more appropriate, the best-fit power law equation is used for this study because it is simple and flexible. Because Luco and Cornell (2001) demonstrated that a nonlinear regression analysis in the form of the power law equation may be used, further investigation on possible best fit equations is not performed.

The best-fit power law equation in this thesis is found using a conditional variance where the variance is assumed to be constant. One other way to determine the best-fit power law equation is by means of the least squares method. Both methods are used to find the equations that relate seismic intensity to structural demand for the original structure using spectral acceleration. The equation used in Chapter 3 using a conditional variance is shown again in Equation 4.4 to compare with the equation found using the least squares regression procedure as shown in Equation 4.5. The demand

uncertainty values for each equation are also shown below each regression equation. The demand uncertainty using the conditional variance method is found to be smaller than the least squares method and therefore, the conditional variance method will be used in this thesis.

$$Y_{p_{Sa}} = 4.5451 S_a^{0.8653}$$
$$\beta_{D|S_a} = 0.0909$$

(4.4)

$$Y_{p_{Sa}} = 4.4897 S_a^{0.8483}$$
$$\beta_{D|S_a} = 0.0947$$

(4.5)

Fragility curves using the two equations were evaluated to determine the impact of using different methods to determine the best-fit equation. Figure 4.1 shows the comparison of the fragility curves using Equation 4.4 and Equation 4.5. Figure 4.2 shows a zoomed-in section to show that the slight difference between the curves is negligible.
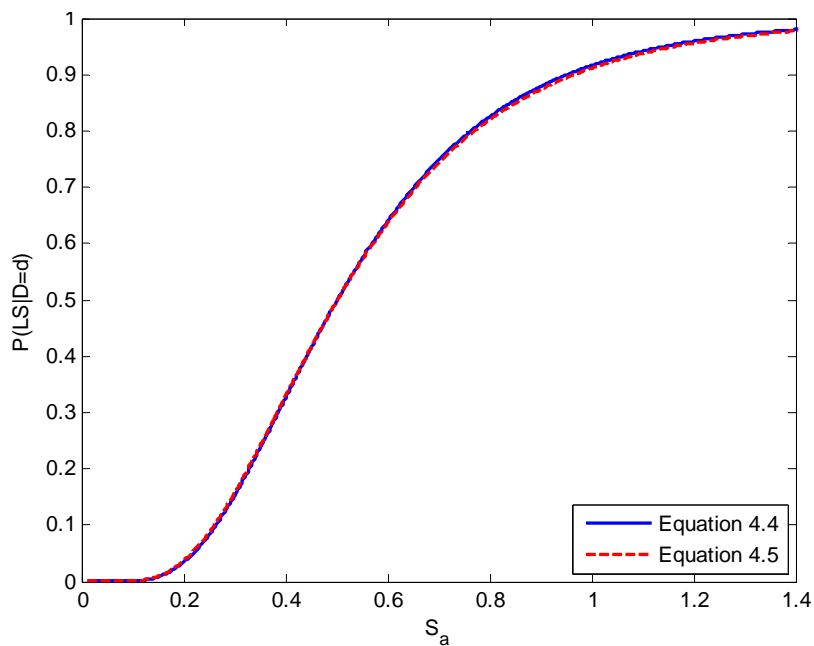

Figure 4.1 Effects of Different Best-fit Curves on the Fragility Curve

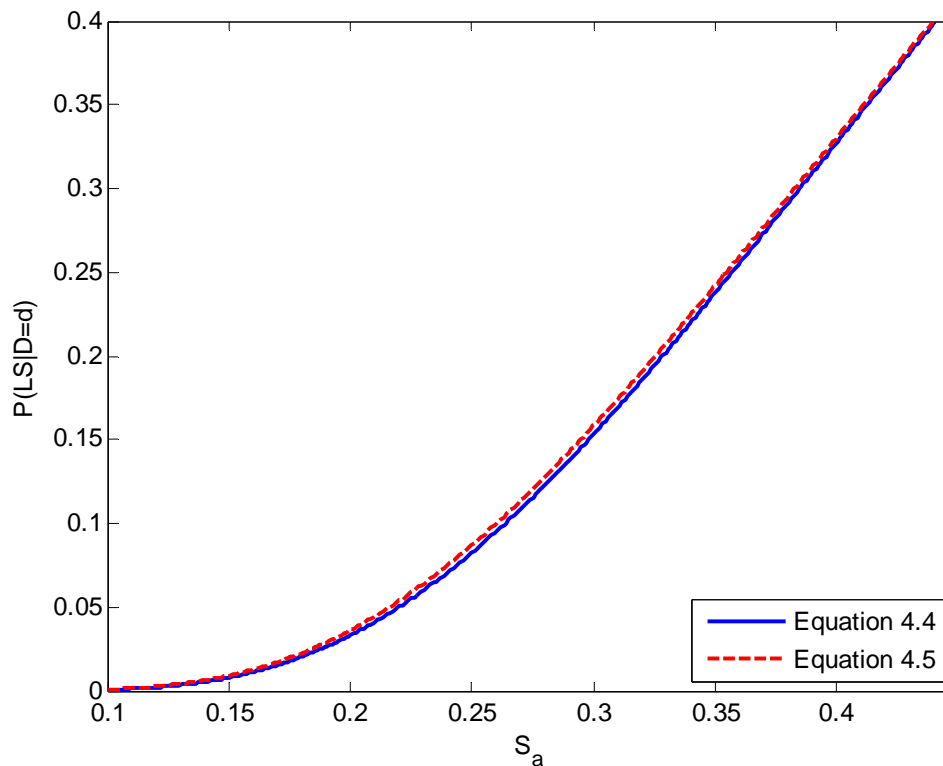**(β_c=0.3 and β_m=0.3) using Life Safety Limit State**

Figure 4.2 Effects of Different Best-fit Curves on the Fragility Curve
(β_c=0.3 and β_m=0.3) using Life Safety Limit State (Zoomed In)

To reduce the amount of error, many earthquake records should be used to determine the best fit power law equation. However, for ground records from Memphis, TN, Wen and Wu (2001) demonstrated a small coefficient of variation (<10%) of the median response for both linear and nonlinear inelastic systems from ten uniform hazard ground motions compared to using large (9000) samples. Therefore only ten ground motions were selected from the multiple developed simulations for a city to most accurately match the uniform hazard response spectra at two different exceedance probabilities, 2% and 10% in 50 years hazard level. Due to this small variation, ten ground motions are assumed to be an efficient number of records because a large number of ground motions would be computationally expensive for a small reduction in demand uncertainty. Twenty time history analyses are simulated from the ten ground motion records of two exceedance probabilities so *n* is equal to twenty for this study.

Although a structure's natural period is needed, spectral acceleration is the most commonly used intensity measure in practice (Baker and Cornell 2006). Therefore, spectral acceleration is used as the main intensity measure of seismic ground motion for this study, but other intensity measures could be used such as peak ground acceleration (PGA), peak ground velocity (PGV), or modified Mercalli intensity. When spectral acceleration is used as the intensity measure, Equation 4.2 determines the uncertainty of the demand is 0.091. However, when PGA is the intensity measure, the demand uncertainty is 0.269. Less uncertainty is present when spectral acceleration is defined as the intensity measure because spectral acceleration is a building specific intensity measure and is more correlated to the structure's response.

4.3   Modeling Uncertainty

Wen et al. (2004) and Bai (2004) have used a value of 0.3 for both the capacity and modeling uncertainties (β_{CL} and β_M). To examine the influence of modeling uncertainty on the fragility analysis, the capacity uncertainty is first defined as zero. From the power law predicted demand drift equation, the demand uncertainty is found to be 0.091 when spectral acceleration is used as the intensity measure. The modeling uncertainty is varied from 0 to 0.5 and the results are plotted in Figure 4.3.
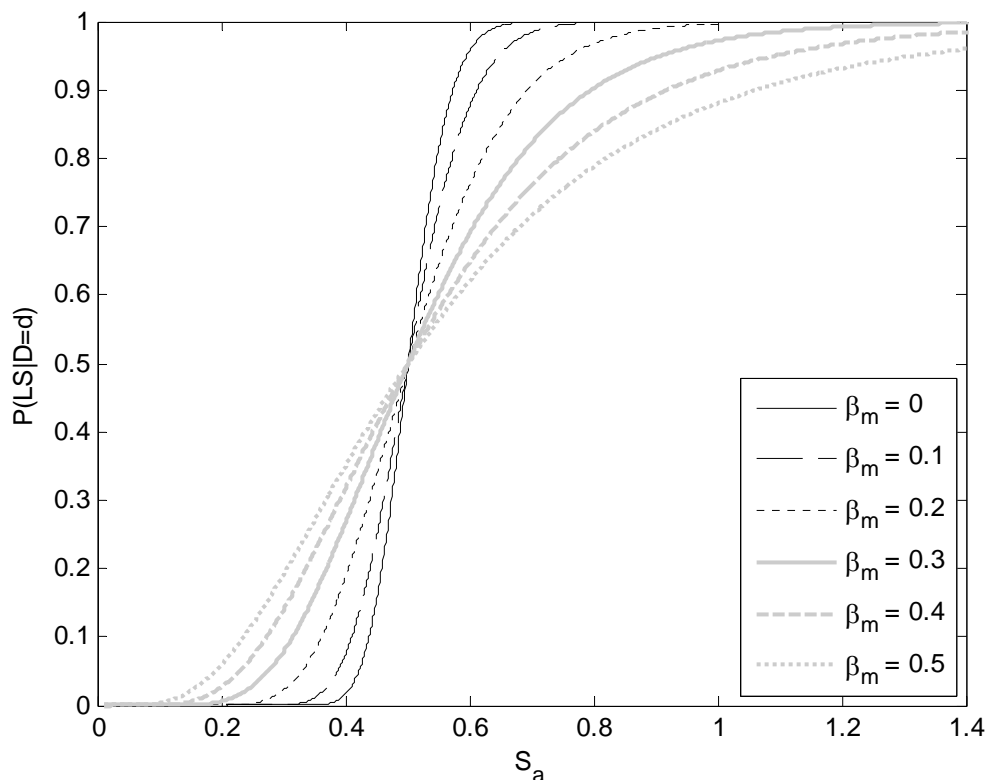
Figure 4.3 Effects of Modeling Uncertainty on the Fragility Curve ($\beta_c=0$)

Figure 4.3 demonstrates that the middle value of the fragility curve is controlled by the capacity of the system and the slope of the curve is controlled by the uncertainty. When the modeling and capacity uncertainties are equal to zero (illustrated as a black solid line in Figure 4.3), the fragility curve is almost a vertical line because the only uncertainty included in the fragility equation is the small demand uncertainty from the power law equation. The large modeling uncertainty range from 0% to 50% produces a large variation in results. Figure 4.4 shows a smaller range of values for the modeling uncertainty with the assumption of zero capacity uncertainty. The differences between specific values of modeling uncertainty within a small reasonable range are shown not to be significant to the overall shape of the curve. Wen et al. (2004) also compared the results of modeling error and concluded that a value of 30% modeling error is an reasonable value to be defined for use in future fragility studies within the MAE Center (Wen et al. 2004). Therefore, for the use of this study the value of $\beta_M =0.3$ is used to

account for the uncertainty in the simulation programs, the integration schemes, and the modeling of the nonlinear materials.
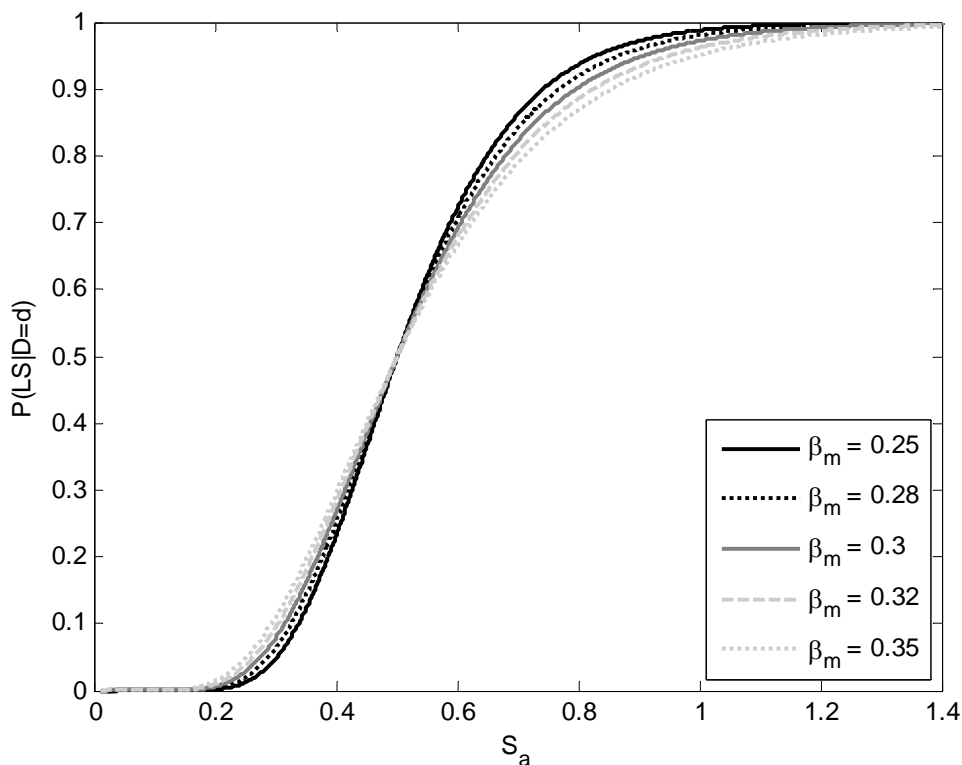

Figure 4.4 Effects of a Small Range of Modeling Uncertainty on the Fragility Curve (β_c=0)

4.4   Capacity Uncertainty

Wen et al. (2004) demonstrated that the "uncertainty in steel frame capacity, measured by β_{CL}, has only a marginal impact on seismic risk" and "minor changes in β_{CL} may have a negligible impact on limit state probability for seismic events in the Eastern United States."   For modeling uncertainty equal to 0.3 and demand uncertainty determined as 0.091 using spectral acceleration, capacity uncertainty is varied from zero to 0.5 as shown in Figure 4.5. FEMA 356 defines inter-story drift values that are typical values of the overall performance of the structure associated with a particular performance level, but inherent uncertainties cause variation between the model and the

structure's performance (FEMA 2000). Therefore, the difficulty arises in determining an appropriate value for the capacity uncertainty. A value of 50% is a large value for the capacity uncertainty and zero uncertainty in not realistic. A smaller range of capacity uncertainty values is shown in Figure 4.6 and the effect of a smaller range in the capacity uncertainty can be seen as negligible. For use of FEMA defined limit states using inter-story drift limits, the uncertainty parameter β_{CL} has been investigated and validated as 0.3 by Wen et al. (2004) and therefore $\beta_{CL} = 0.3$ will be used in this thesis.
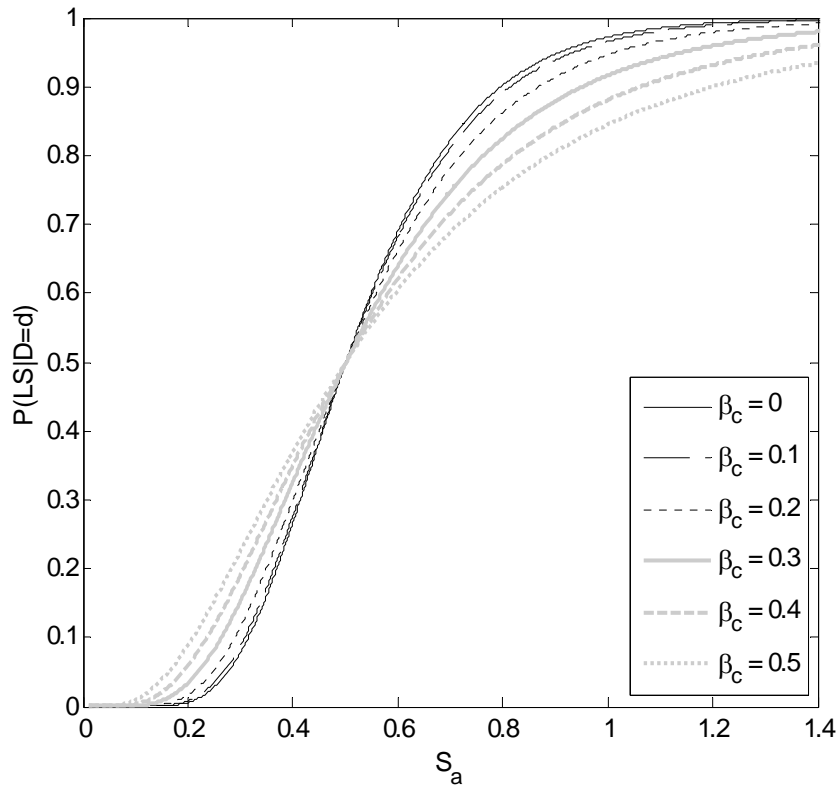

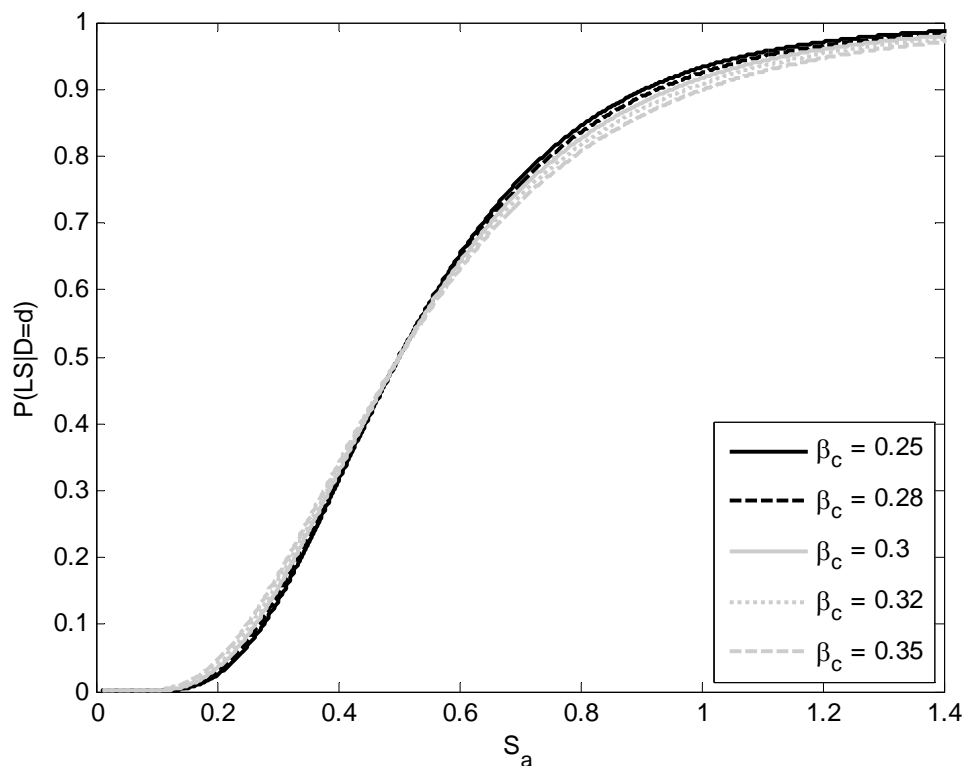**Figure 4.5 Effects of Modeling Uncertainty on the Fragility Curve (β_m=0.3)**

Figure 4.6 Effects of a Small Range of Modeling Uncertainty on the Fragility Curve (β_m=0.3)

4.5   Summary

This chapter summarizes the effects of the uncertainty on a fragility analysis. The demand uncertainty parameter is shown to be reduced when spectral acceleration is used as the intensity measure. The best fit law determined from using a variable variation produces less uncertainty. The modeling and capacity uncertainty values are varied and the effect of large and small ranges is presented. At small ranges, the shape of the fragility curve is very similar. Larger uncertainty values cause the probability of failure to be greater at small earthquake intensity levels and smaller at larger uncertainty values. The uncertainty affects the slope of the fragility curve and does not affect the middle value. Wen et al. (2004) have investigated the values of uncertainty and have determined that 0.3 is an acceptable value for the modeling and capacity uncertainty values for MAE Center projects. The modeling and capacity uncertainty values are

defined as 0.3 for this study to account for epistemic and aleatory sources of uncertainty in the nonlinear behavior of the structure.

Chapter 5

Fragility of Structure with Passive Devices

Building owners often seek to reduce the fragility or vulnerability of their structures. Although many retrofit options exist, this study focuses on the options of adding control of passive and active systems. The reasons for selecting passive control devices include their inherent stability and make them a desirable option for retrofit. This chapter focuses on the development of fragility curves for a structure with passive control devices. Passive dampers are integrated into chevron braces for this study. Two device placements are proposed with one designed using engineering judgment and the other using an optimal placement technique with fewer devices. The control design placement of two device configurations is discussed and the fragility curves of both placements are presented. A comparison of the vulnerability between the two placements is also included.

5.1 Device Model and Placement

The analytical model of the three-story steel moment frame structure considered in this thesis is discussed in Chapter 3. To improve the responses of the structure under seismic excitations, passive devices are added to the frame to increase damping of the system. Two device placements are investigated.

Before the device configurations and models are discussed, a few implementation issues should be addressed. Several ways to compare two control systems exist, but in each

case one parameter is chosen to be similar between the systems to allow a comparison of the other variables in the system. A couple possibilities for designing comparable systems include matching the maximum force of a single device or the sum of the maximum forces in all the devices for a specified earthquake record. Although maximum force determines the necessary size of a device, the total control effort (or force) is also an important factor to consider especially for an active system that requires power. Power outages are common during severe earthquakes and the amount of generated power necessary for a controlled system is often a design consideration. The approach in this study is to compare the sum of the squares of the control force variance for the duration of a design earthquake record. One other design consideration should be noted; the control systems described in this thesis are designed using a linear system, but the responses used for the fragility analysis must be found using a nonlinear dynamic analysis. As such, the performance of the control systems in a nonlinear analysis may differ from a linear analysis, but the forces are designed to be similar in the linear and nonlinear analyses.

5.1.1 Placement A Using Engineering Judgment

Engineering judgment is often used when designing a structure or control system because the time necessary to determine an optimal solution is possibly more costly than just using an assumed suboptimal solution. The first device configuration considered here uses engineering judgment to place six devices in chevron braces as shown in Figure 5.1 and has been a commonly adopted control configuration for several research studies. This device configuration will be referred to as Placement A hereinafter.
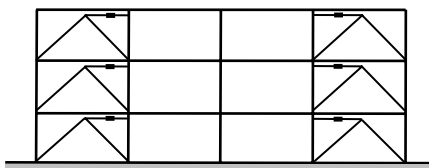

Figure 5.1 Chevron Brace Configuration for Placement A

Once the device placement has been decided, the control algorithm and device size can be determined. The passive devices used in this study are assumed to be ideal viscous dampers that add linear, velocity-proportional damping to the structure. The damping ratios of the first two modes of the structure are $\zeta_1 = \zeta_2 = 0.02$ as discussed in Chapter 3. One design objective is to increase the damping of the first mode from 2% of the original structure to 9% of the passive controlled structure. The more the damping ratio is increased, the more force is required from the passive damper. For Placement A, all devices are selected such that they have the same properties, making the damping coefficient in Equation 2.5 associated with each device equal. A range of damping coefficients is evaluated to determine an appropriate value that achieves the design objective. The force each device provides to the structure is also considered because the maximum control force directly relates to the cost of the device. When the damping coefficient is equal to 500 for each device, the damping of the first mode is 0.0891. The maximum force is restricted to be under 500kN.

The additional force from the passive dampers is included with the inertial and damping forces to determine the total force at each node in UI-SIMCOR. ZeusNL determines the restoring force from the stiffness of the structure.

5.1.2   Placement B Using Optimal Placement

The previous section considered using engineering judgment to place six devices in the moment-resisting frame. The structure contains two moment resisting frames so a total of twelve devices are necessary for Placement A. It is desirable to decrease the number of devices in a structure to reduce the cost of control. Optimal placement can determine the most advantageous placements for a specified number of devices. One design objective for the second device placement configuration is to reduce the number of devices to two per frame with a total of four devices in the structure such that the control configuration will include fewer devices than number of floors per frame. Optimal placement will determine which floors control braces should be placed to

reduce the responses of the structure the most. The relationship between the control cost and the reduction of probability of failure will be considered.

Twenty-one possible locations for devices are cnsidered. Figure 5.2 shows the number corresponding to each possible placement. Note that for illustration purposes only the chevron braces are depicted as diagonal braces.
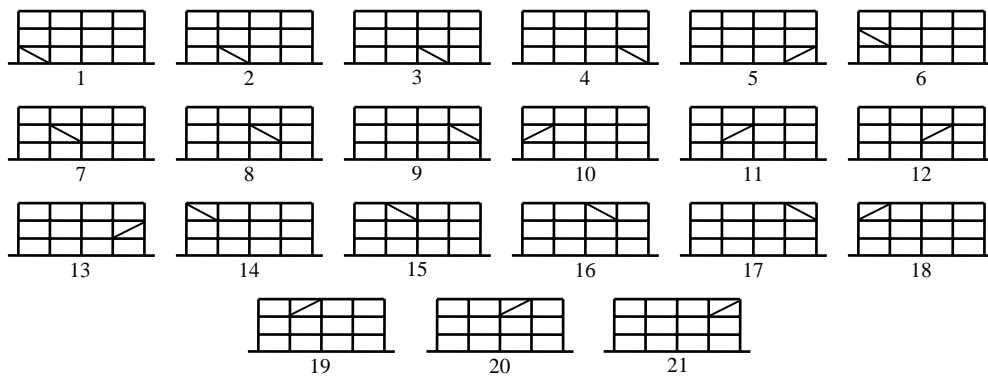

Figure 5.2 Possible Device Placements

The theory of optimal placement based on Hankel norms is explained in Section 2.3.2. The device placement indices are found for each of the possible locations and shown in Figure 5.3. Only the first three modes are considered because they should dominate the displacement responses of the structure and thus have the largest impact on the fragility. Figure 5.4 shows placement indices for the modes at each story level. To reduce the response of the first mode, devices should be placed on the second story. However, devices on the second story have only a small effect on the second mode. The second mode is best controlled by devices placed on the third story.
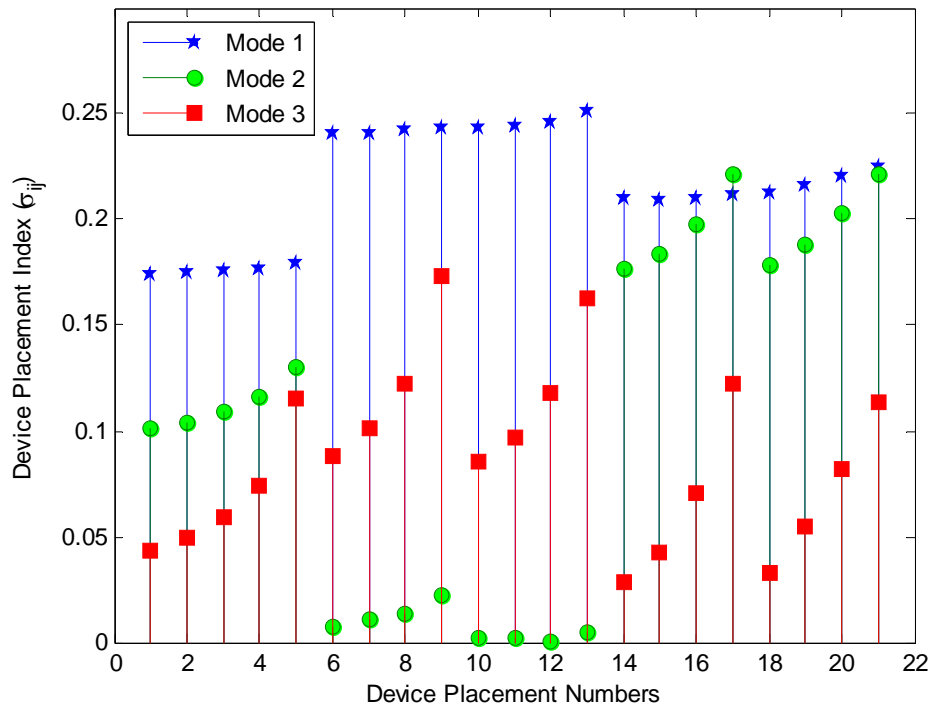
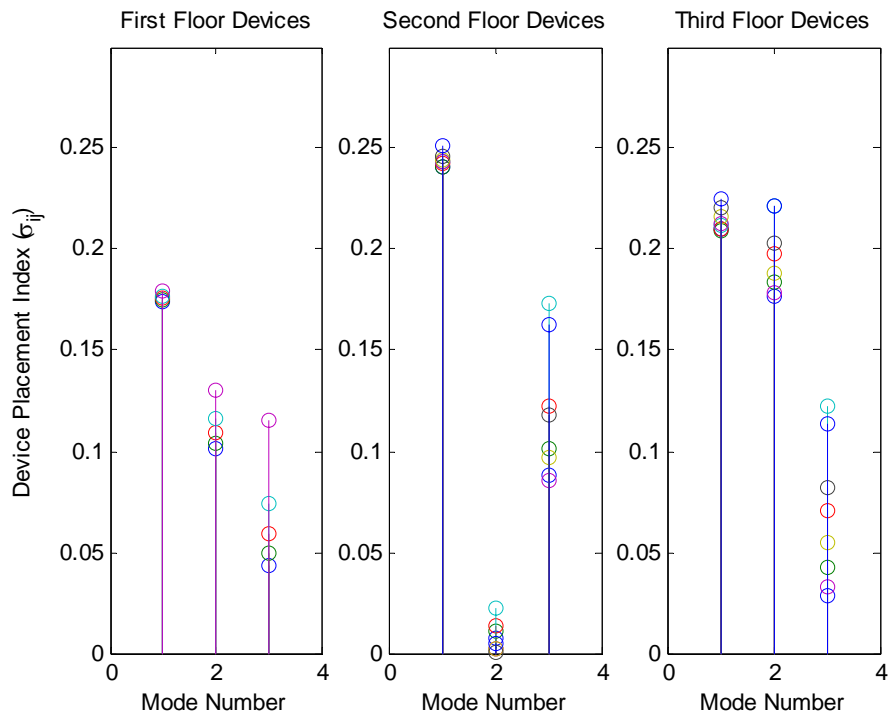**Figure 5.3 Control Device Placement Index**

Figure 5.4 Device Placement Index for Each Mode

One design objective is to reduce the number of devices to two devices in the second configuration or Placement B. Highly correlated placements are excluded and device locations 9 and 21 from Figure 5.2 are chosen as the optimal placement to reduce the first and second mode responses. The optimal placement configuration shown in Figure 5.5 will be referred to as Placement B hereinafter.
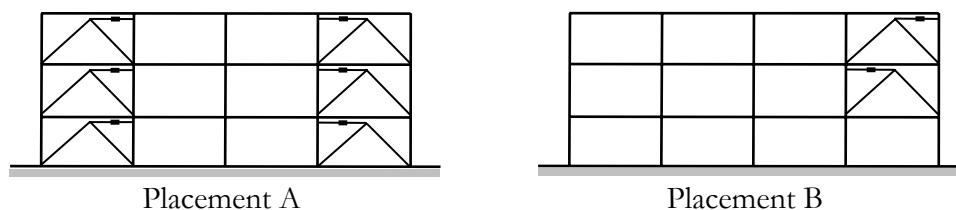

Placement A   Placement B

Figure 5.5 Device Placement Configurations

Once the device placement is decided, a range of damping coefficients is considered to satisfy a design objective. For purposes of comparison, the optimal active control case was first designed and then the square root of the sum of the squares of the required force variance is used as a design objective for the optimal passive controlled system. This approach allows for direct comparison of passive and active systems with matching control efforts. This design objective is discussed in further detail in Section 6.1.2. The damping coefficient is determined to be 390 for each device and, using this value, the force of each device does not exceed 400kN for the twenty ground motion records.

5.2   Fragility Curves of the Passively Controlled System

The procedure to develop a fragility curve that is outlined in Chapter 3 is implemented here on the two passive controlled systems. To facilitate a comparison of the results of the passive controlled structure with the original structure, the ground motions used for both evaluations are synthetic ground motions of Memphis, TN with representative soil developed by Wen and Wu (2001). The natural frequencies of the structure with

control devices are assumed to be equal to the natural frequencies of the structure without control devices. The additional mass of the devices is assumed to be negligible compared to the seismic mass of the structure and the assumption of viscous damping neglects additional stiffness to the system. Therefore, the spectral acceleration of each ground motion record which uses the fundamental frequency of the structure is assumed to be identical for the controlled and the original structure. Once the ground motions are identified, the analytical models of the structure and the control system are defined. The analytical models of the structure and the passive devices are described in Section 3.2 and Section 5.1, respectively.

5.2.1   Passively Controlled Fragility Curves (Placement A)

The responses of the controlled structure with passive devices arranged as in Placement A from the twenty ground motion records are determined from nonlinear time history dynamic analyses. The maximum transient interstory drifts at each story level are shown in Figure 5.6 and the permanent drifts from the nonlinear analysis are shown in Figure 5.7. For the earthquake representing a 10% exceedance level in 50 years, the structure undergoes small transient drifts and does not experience permanent deformations so the assumption that the structure is behaving linearly could be made. Nonlinear behavior can easily be seen based on the permanent drifts from the higher intensity earthquake records.

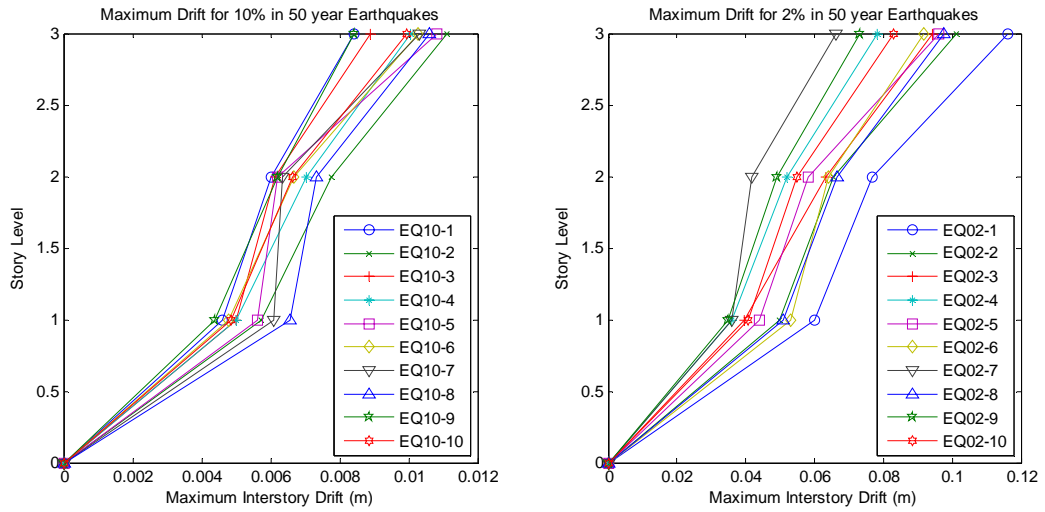**Figure 5.6 Maximum Interstory Drift for the Passively Controlled Structure (Placement A)**
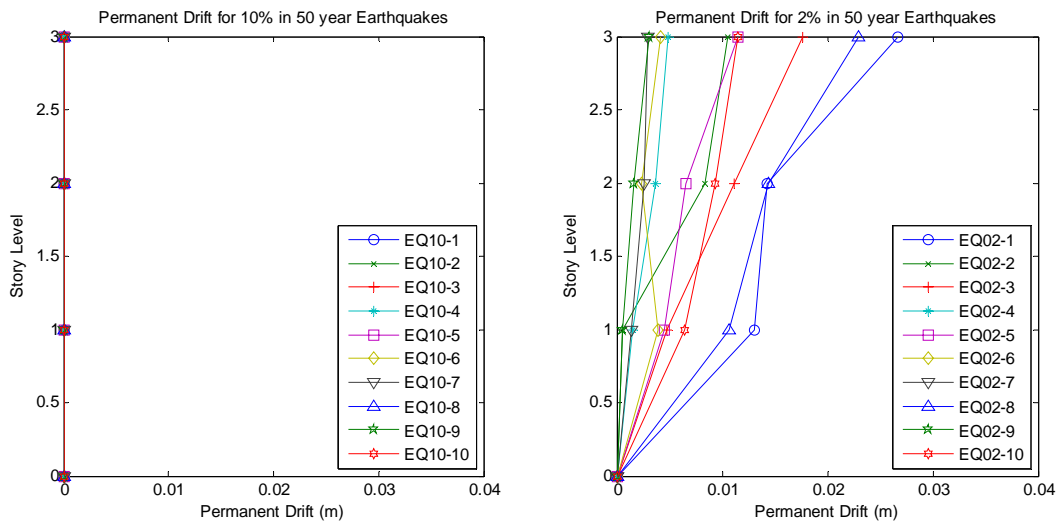

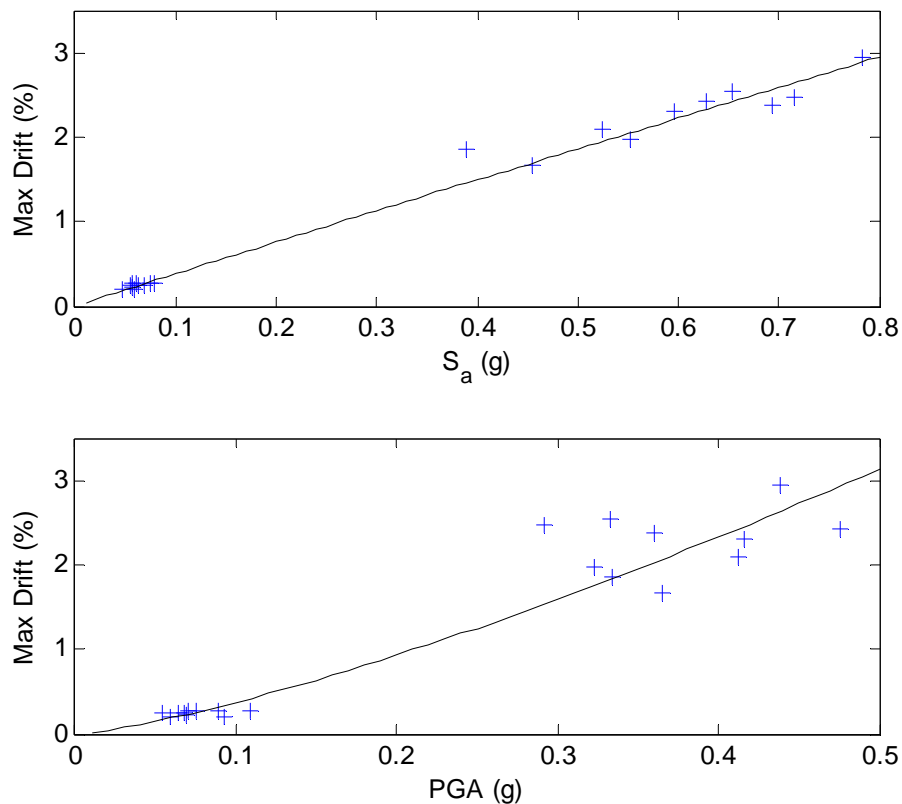**Figure 5.7 Permanent Interstory Drift for the Passively Controlled Structure (Placement A)**

The maximum drift of each ground motion record is plotted against the record's demand as shown in Figure 5.8. The two best fit power law equations are calculated as

$$Y_{P_{S_a}} = 3.662 S_a^{0.9772}$$
$$R^2 = 0.9882$$

(5.1)

$$Y_{P_{PGA}} = 7.8036 \text{PGA}^{1.3207}$$

$$R^2 = 0.9511$$

(5.2)

Figure 5.8 Probabilistic Seismic Demand Model for the
Passively Controlled Structure (Placement A)

Using Equation 3.5, a fragility curve is plotted in Figure 5.9b using spectral acceleration as the intensity measure for three different limit states: immediate occupancy (IO), life safety (LS), and collapse prevention (CP). For comparison, the fragility curves for the original structure are also shown. When the intensity measure is $S_a=0.6g$, the probability of exceeding the collapse prevention limit state for the original structure is over twice the original structure. For the life safety limit state, the passively controlled system reduces the probability from 65% of the original structure to 40%. However, at $S_a=0.6g$ the immediate occupancy level is almost guaranteed to be exceeded for both the original and passively controlled structures. A fragility analysis is decoupled from the

ground motion probability. However, for reference, Figure 5.9a compares the intensity level to the probability of exceedance in 50 years. Note the 2% probability of exceedance in 50 years is roughly a spectral acceleration of 0.6g. A best fit power law equation is found to depict the relationship between the probability of exceedance and the intensity level. Note that the study of probability of earthquake occurrences is beyond the scope of this study the best fit equation is provided for visualization, but may not be appropriate for other uses.

A system demand displacement curve is shown in Figure 5.10 as a different way to show the vulnerability of the structure. Note that life safety limit state for a steel moment-resisting structure is 2.5% transient interstory drift and therefore, the probability of exceedance in 50 years is less than 2% when occurrence uncertainty is not included. Note that the system demand displacement curve in Figure 5.10 does not consider uncertainty in the system so a fragility curve is a more accurate representation of the vulnerability of the system.

(a) Probability of Exceedance of Memphis, TN Ground Motions

(b) Fragility Curve for 3-Story Steel Building
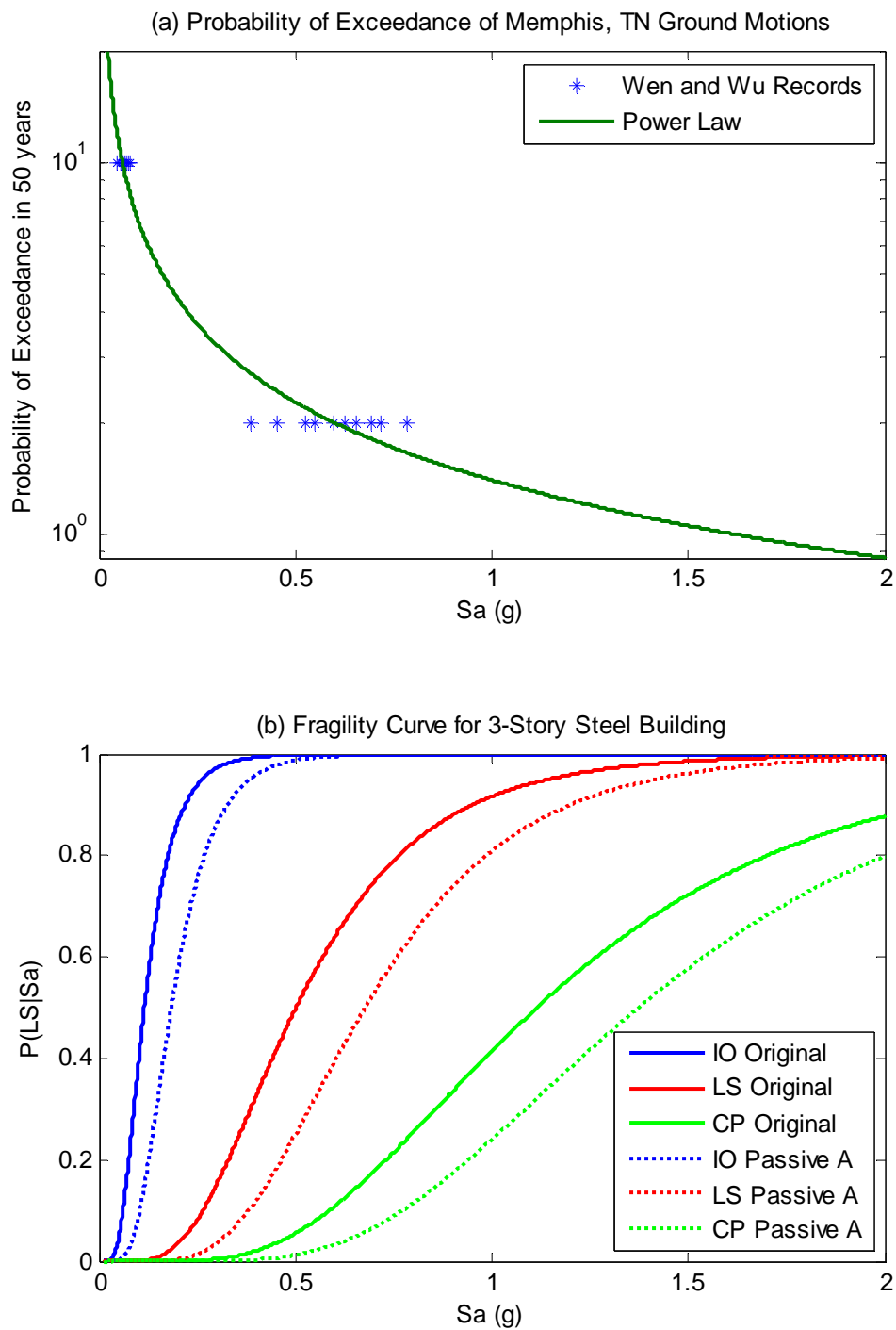
Figure 5.9 Fragility Curve of Passively Controlled Structure (Placement A)
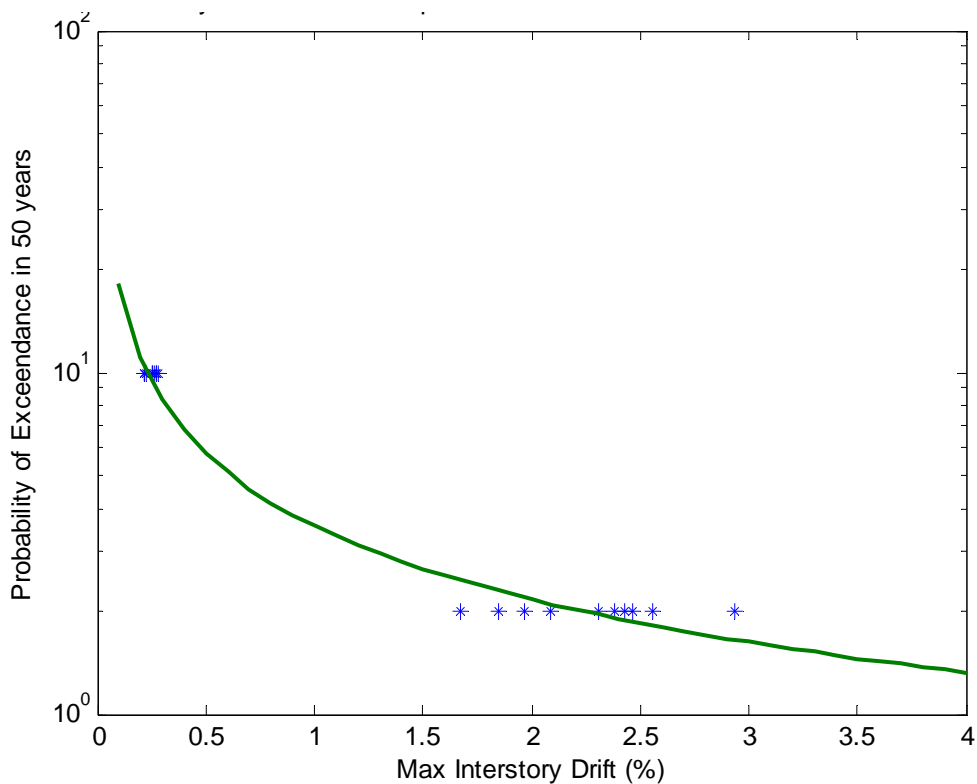
Figure 5.10 System Demand Displacement Curve with Passive Control (Placement A)

5.2.2   Passively Controlled Fragility Curves (Placement B)

The responses of the controlled structure with optimally placed passive devices from the twenty ground motion records are determined from nonlinear time history dynamic analyses. The maximum transient interstory drifts at each story level are shown in Figure 5.11 and the permanent drifts from the nonlinear analysis are shown in Figure 5.12. As with Placement A, the structure does not experience permanent deformations for the 2% in 50 years exceedance ground motion records.
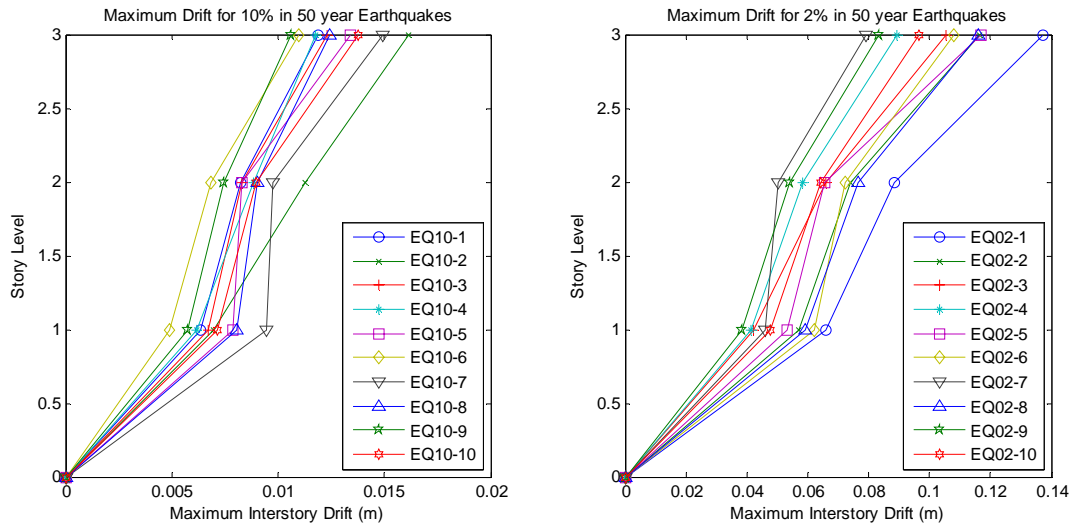
Figure 5.11 Maximum Interstory Drift for the Passively Controlled Structure (Placement B)
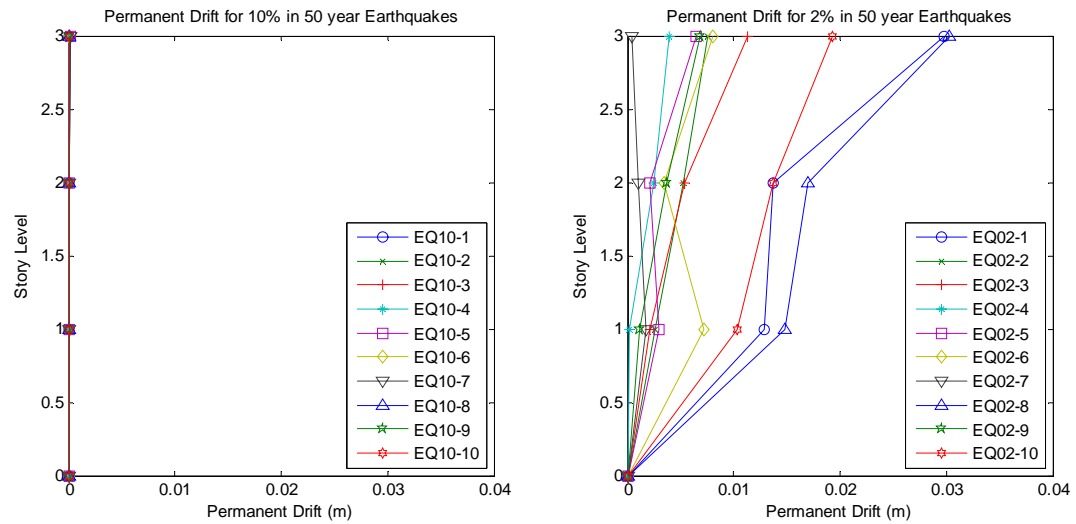
Figure 5.12 Permanent Interstory Drift for the Passively Controlled Structure (Placement B)

The maximum drift of each ground motion record is plotted against the record's demand as shown in Figure 5.13. The two best fit power law equations for Placement B are calculated as

$$Y_{P_{S_a}} = 4.2558S_a^{0.9243}$$

$$R^2 = 0.9956 \tag{5.3}$$

$$Y_{P_{PGA}} = 8.6032PGA^{1.2427}$$

$$R^2 = 0.9484 \tag{5.4}$$
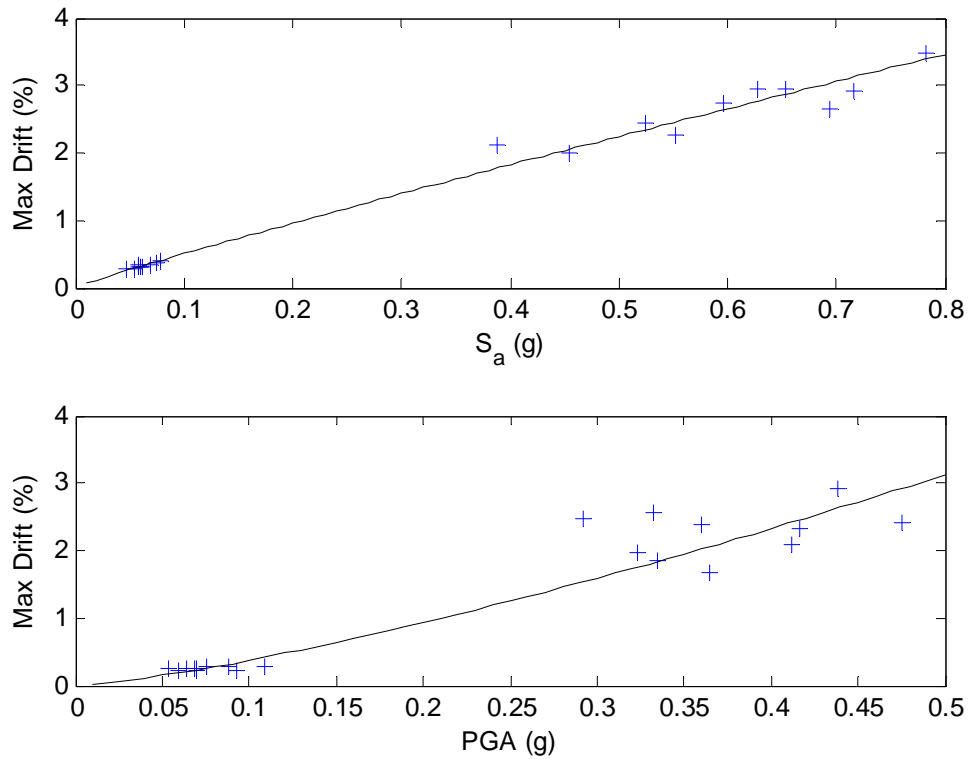
Figure 5.13 Probabilistic Seismic Demand Model for the

Passively Controlled Structure (Placement B)

(a) Probability of Exceedance of Memphis, TN Ground Motions

(b) Fragility Curve for 3-Story Steel Building

Figure 5.14 Fragility Curve of Passive Controlled Structure (Placement B)

The fragility curves for placement B is plotted in Figure 5.14b using spectral acceleration as the intensity measure for the three different limit states. For comparison, the fragility curves for the original structure are also shown. At S_a=0.6g, adding only two devices in the frame reduces the probability of exceeding life safety limit state from 65% of the original structure to 55% of the passive controlled structure and reduces the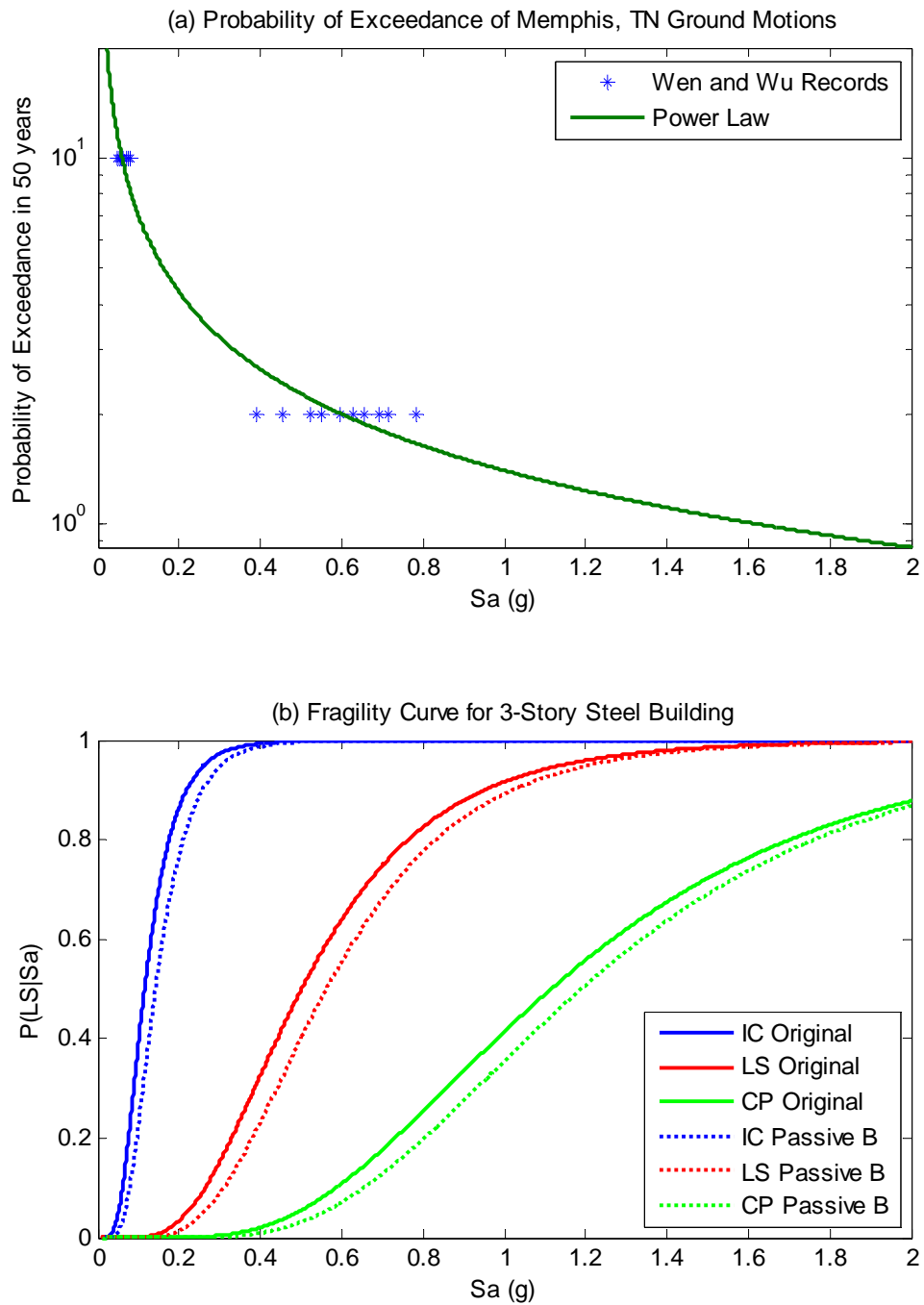 collapse prevention limit state from 11% to 7%. Again Figure 5.14a provides a visual comparison of the intensity level to the probability of exceedance in 50 years for Memphis, TN although this may not be appropriate for other uses.

The system demand displacement curve for the passively controlled system in placement B is shown in Figure 5.15. Note that life safety limit state for a steel moment-resisting structure is 2.5% transient interstory drift which corresponds to the probability of exceedance in 50 years of about 2% when uncertainty is not included. As discussed earlier, the system demand displacement curve does not consider uncertainty in the system and care should be taken when decision making with a system that does not consider uncertainty.
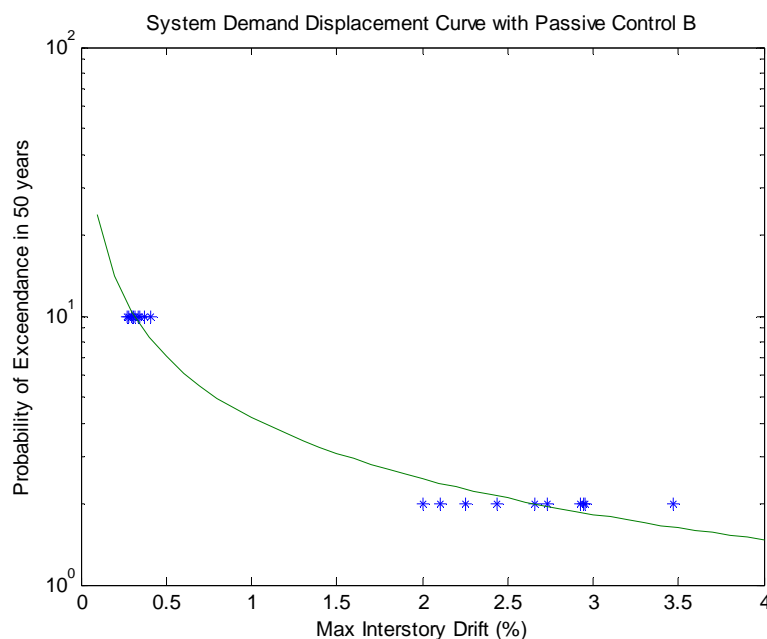
Figure 5.15 System Demand Displacement Curve with Passive Control (Placement B)

5.2.3 Comparison of Passive Placement A and B

A comparison between the two device configurations is performed to investigate the differences in responses between systems with six devices compared to a system with two devices. Figure 5.16 shows the fragility curves for placement A and placement B of the passively controlled structure along with the original structure for the life safety limit state. Both passive systems decrease the probability of failure. Placement A decreases the probability of exceeding the life safety limit state more so than placement B, but one should expect a greater decrease in response when more devices are used. When the spectral acceleration is equal to 0.6g, the probability of failure of the original, passive case A, and passive case B are 65%, 40%, and 55%, respectively. Although placement A shows a dramatic drop in fragility, placement B also has roughly a 15% decrease in the probability of meeting or exceeding the life safety limit state compared to the original structure. This performance gain is achieved at approximately one third the cost of the design using placement A.
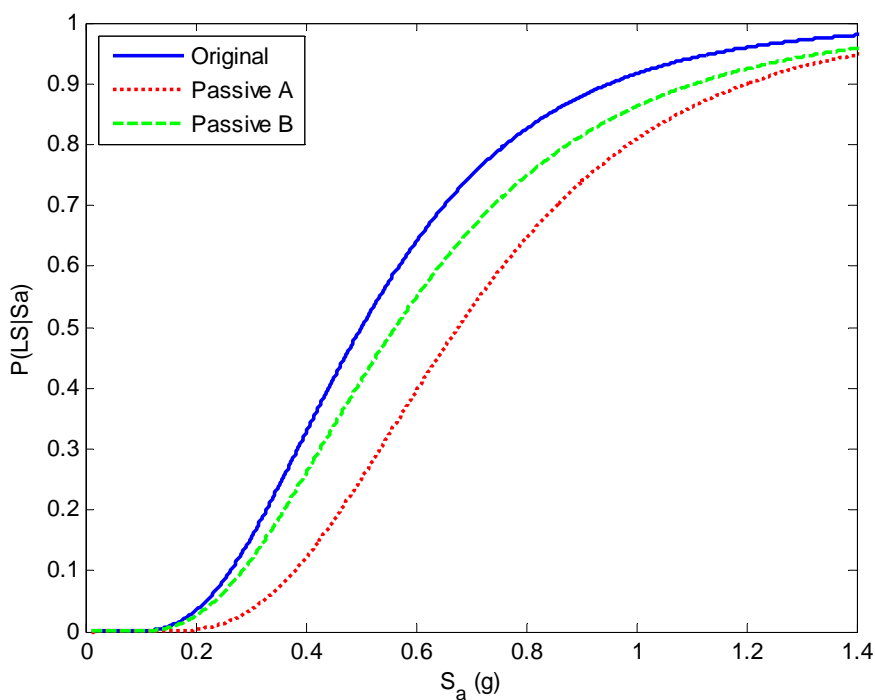
Figure 5.16 Passively Controlled Fragility Curves for Placement A and Placement B (Life Safety)

5.3   Summary

The development of fragility curves for passive systems has been demonstrated here. The addition of passive devices has been shown to considerably reduce the vulnerability of the steel moment-resisting structure. Two device placements have been considered with one configuration chosen using engineering judgment (placement A) and the other configuration found using optimal placement techniques. The optimal configuration (placement B) has a reduced number of devices, only two devices per frame compared to six devices of placement A. For the life safety limit state and when the spectral acceleration is equal to 0.6g, the probability of failure of the original structure is 65% compared to 40% and 55% of passive case A and passive case B, respectively. A greater number of devices reduced the fragility significantly more than the optimal configuration. However, the additional cost of using three times the number of devices should be considered when comparing the reduction of vulnerability.

Chapter 6

Fragility of Structure with Active Devices

This chapter focuses on the development of the fragility of a structure with active control. Active control uses actuators to input a control force to the structure that is determined from a control algorithm that considers the structural responses and therefore, is able to adapt to changing environments. Performance of active systems depends on the control objectives and control algorithm. The two device placements described in Chapter 5 are used with active devices and the fragility curves of the actively controlled systems are compared.

6.1 Device Model and Placement

Chapter 3 describes the analytical model of the three-story building considered in this thesis. One objective of this study is to compare the fragility of the passive systems described in Chapter 5 with active systems. The two device configurations described in Chapter 5 and shown in Figure 5.5 for passive control are also considered for active control. The control devices in this study are modeled as ideal devices. Thus actuator dynamics and control-structure interaction are not included in the device models.

An H_2/LQG control law is used to design the active controller as discussed in Chapter 2. Acceleration feedback is chosen and a Kalman filter is implemented to estimate the states of the system from the measured accelerations. Accelerations are assumed to be measured at the middle of each story. The weighting matrix is varied to determine an

appropriate controller with a reasonable and appropriate amount of required force. All active devices are assumed to have the same properties. A logical way to compare controlled systems is to consider the total amount of control force necessary to achieve the desired performance. The sum of the squares of the total control force is used to design comparable control systems in this study. As discussed in Chapter 5, the control systems are designed using a linear system in MATLAB. Control forces determined from the linear control analysis are used to be sure equivalent designs are compared.

6.1.1   Placement A Using Engineering Judgment

Device configuration A was chosen based on engineering judgment. Six devices are placed in the steel moment-resisting frame. First the passive system is designed. The required control force to achieve the design objective was used to design the active controller. A design earthquake was chosen to compare the square root of the sum of the squares of the control force in a linear simulation. The weighting values in the infinite horizon performance index as defined in Equation 2.8 are varied until a reasonably close value is found between the passive and active cases. The square root of the sum of the squares of the force variance is determined from the linear analysis and confirmed as comparable systems during a nonlinear analysis as well.

The additional force from the active dampers is included within the total force at each node from inertial forces and damping forces in UI-SIMCOR. Within MATLAB the control force is determined using accelerations from the middle of each story and ZeusNL determines the restoring force from the stiffness of the structure.

6.1.2   Placement B Using Optimal Placement

One design objective of this study is to consider the effect on the fragility curve when fewer devices are considered. The optimal device configuration is designed such that there are fewer devices than number of floors. If the number of devices equals the

number of floors in a structure, engineering judgment determines that one device should be placed on each floor for the best configuration. However, if fewer devices than number of stories are used, mathematical formulas can determine the optimal placement of the devices. The reduction from six devices to two devices per frame was chosen. The optimal placement technique described in Section 5.1.2 is used to determine the device configuration. To compare the two device configurations, the weighting values in the infinite horizon performance index are varied to design a comparable system with placement A.

6.2   Fragility Curves of Actively Controlled Systems

The step-by-step procedure to develop a fragility curve is outlined in Chapter 3. Similar to the original and passively controlled systems, synthetic ground motions from Memphis, TN with representative soil developed by Wen and Wu (2001) will be used in the nonlinear time history analyses for both device configuration analyses. Control-structure interaction and the additional mass of the devices are neglected so the spectral acceleration of each ground motion record using the original structure's fundamental frequency is assumed to be the same for the controlled system. Once the ground motions are identified, the analytical models of the structure and the control system are defined. The analytical models of the structure and the active devices are described in Section 3.2 and Section 6.1, respectively.

6.2.1   Actively Controlled Fragility Curves (Placement A)

The responses of the controlled structure from the twenty ground motion records are determined from nonlinear time history dynamic analyses. The maximum transient interstory drifts at each story level are shown in Figure 6.1 and the permanent drifts from the nonlinear analysis are shown in Figure 6.2.
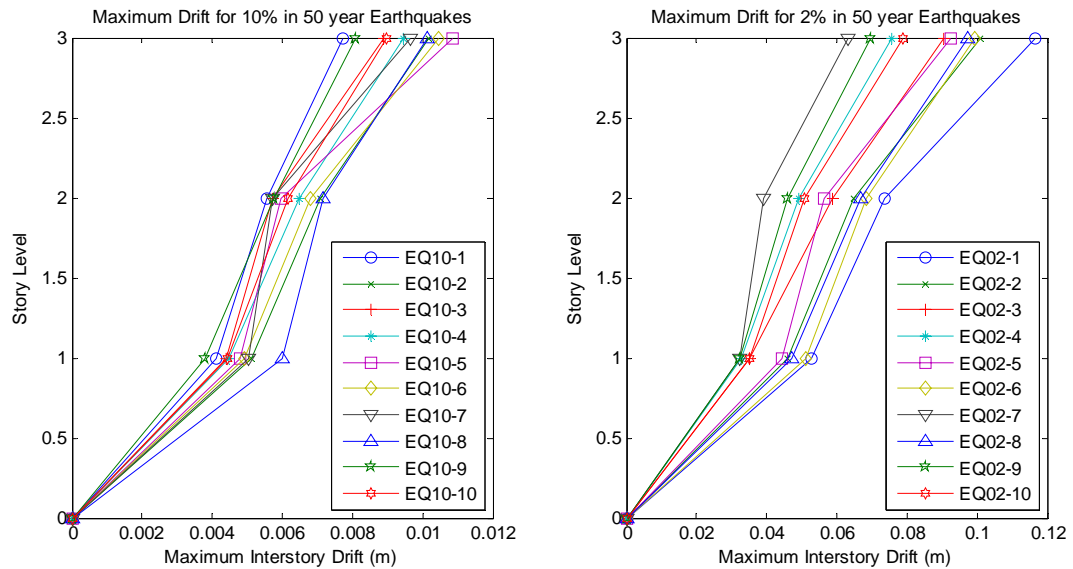
Figure 6.1 Maximum Interstory Drift for the Actively Controlled Structure (Placement A)
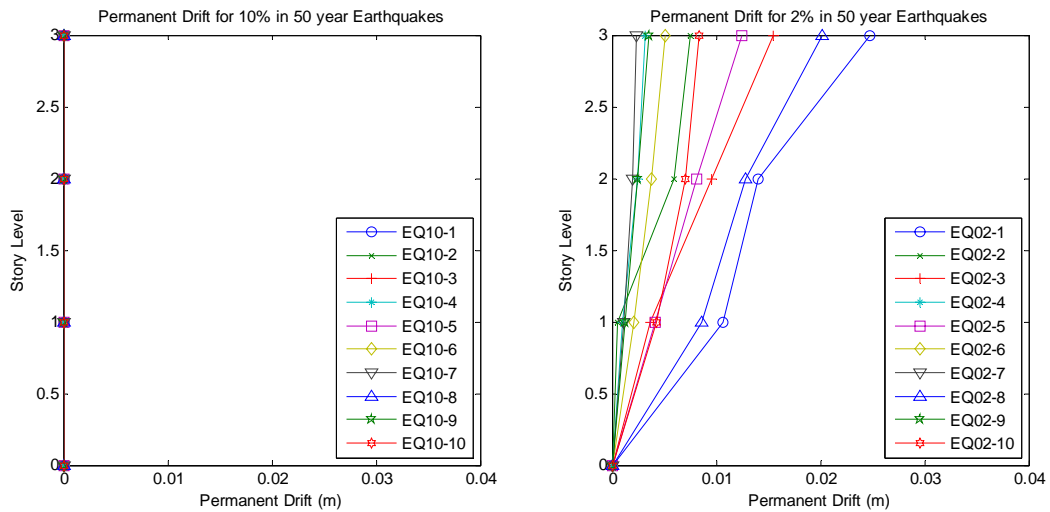
Figure 6.2 Permanent Interstory Drift for the Actively Controlled Structure (Placement A)

A nonlinear regression analysis between the seismic intensity measure and the structural response demand is performed to determine a probabilistic seismic demand model. The probabilistic seismic demand models are shown in Figure 6.3. The power law predicted demand Y_p is determined as

$$Y_{P_{S_a}} = 3.704 S_a^{0.9647}$$

$$R^2 = 0.9919$$

(6.1)

$$Y_{P_{PGA}} = 7.7889 PGA^{1.3018}$$

$$R^2 = 0.9519$$

(6.2)
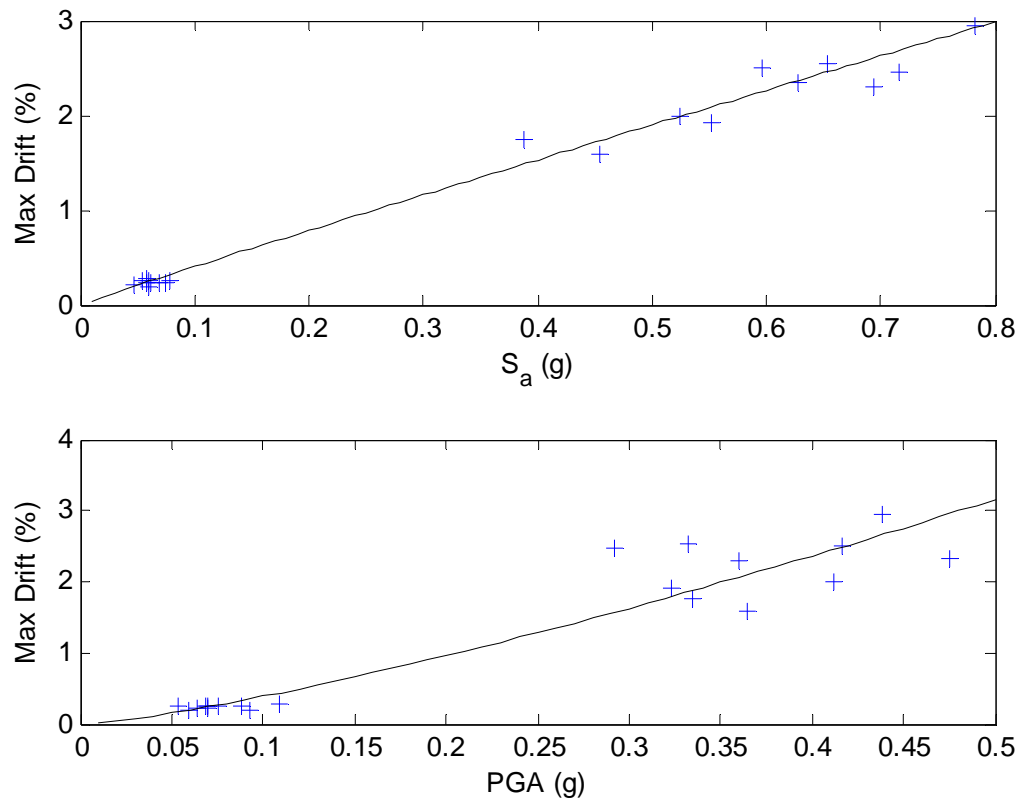
Figure 6.3 Probabilistic Seismic Demand Model for the

Actively Controlled Structure (Placement A)

(a) Probability of Exceedance of Memphis, TN Ground Motions

(b) Fragility Curve for 3-Story Steel Building (Placement A)

Figure 6.4 Fragility Curve of the Actively Controlled Structure (Placement A)

The fragility curves for active controlled placement A is plotted in Figure 6.4b using spectral acceleration as the intensity measure for the three limit states. For comparison, the fragility curves for the original structure are also shown. At S_a=0.6g, adding only two devices in the frame reduces the probability of exceeding life safety limit state from 65% of the original structure to 41% of the actively controlled structure and reduces the collapse prevention limit state from 11% to 4%. Again Figure 6.4a provides a visual comparison of the intensity level to the probability of exceedance in 50 years for Memphis, TN although this power law fit curve is not appropriate for other uses.

6.2.2   Actively Controlled Fragility Curves (Placement B)

Nonlinear time history analyses are performed to determine the maximum and permanent drift for each ground motion record as shown in Figure 6.5 and Figure 6.6. The permanent drift for the smaller intensity ground motion records is negligible and can be assumed that the structure behaves linearly during this time, but nonlinear behavior is shown from the permanent drifts of the 2% in 50 year exceedance intensity level.

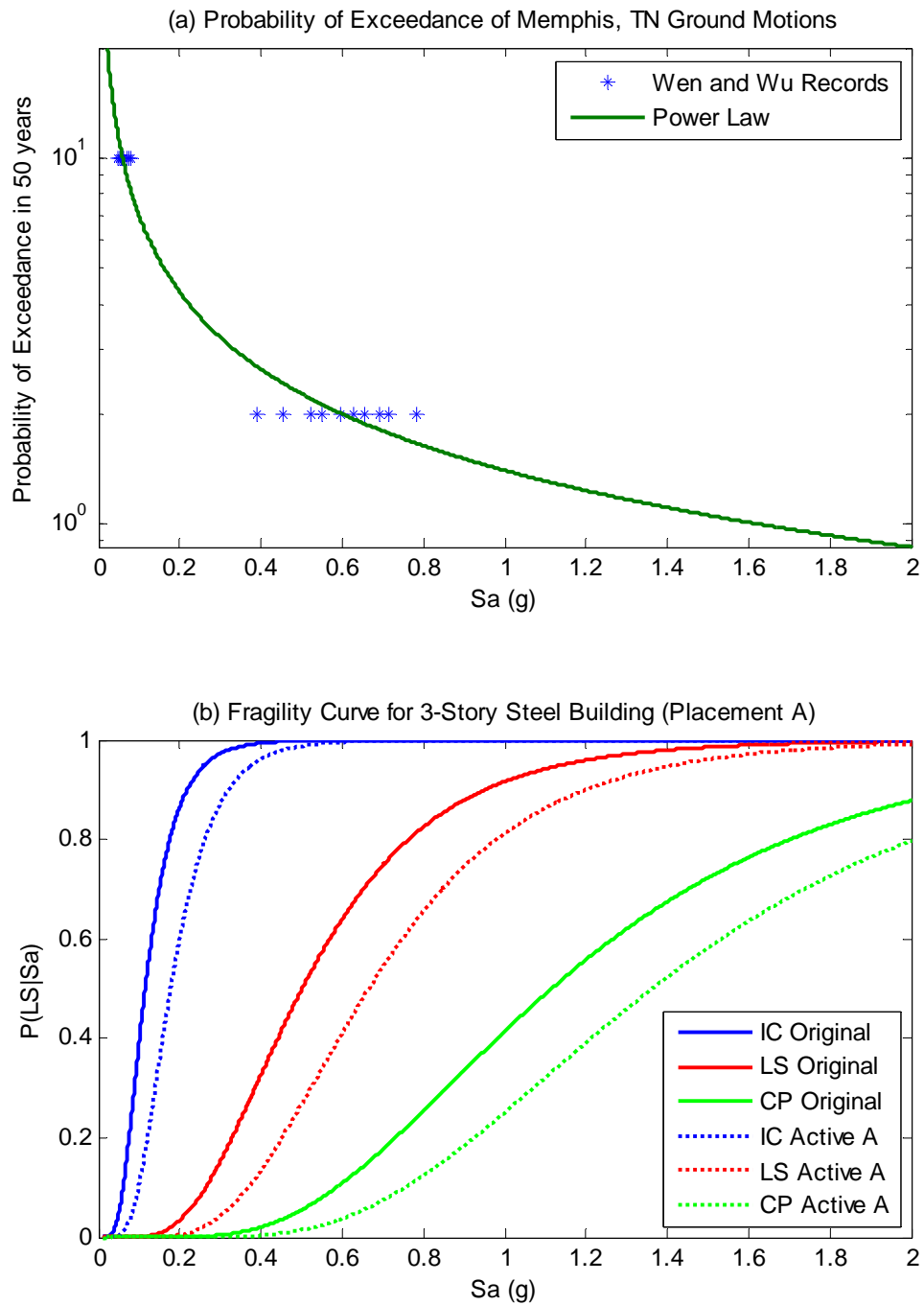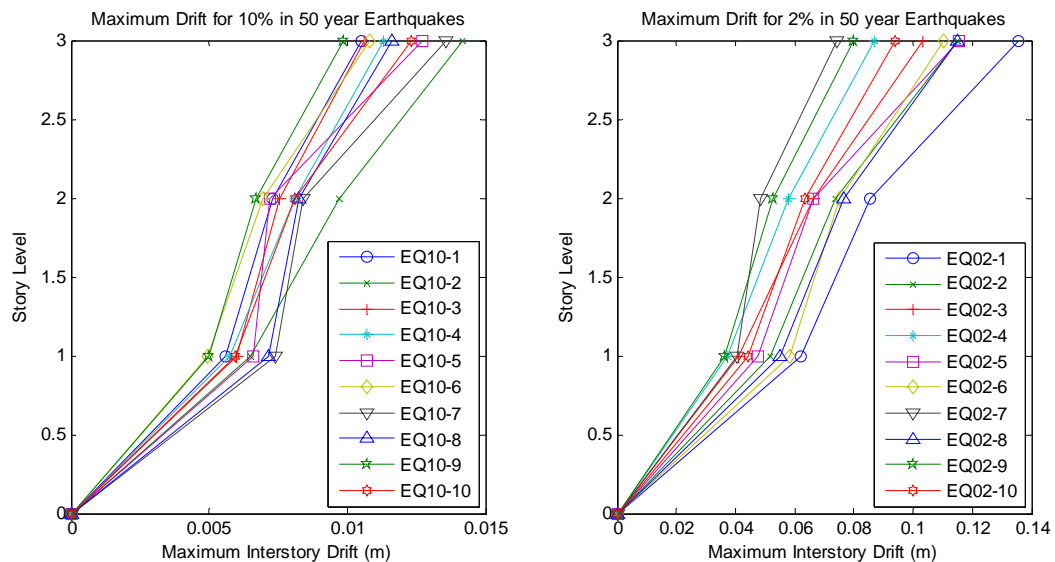**Figure 6.5 Maximum Interstory Drift for the Actively Controlled Structure (Placement B)**
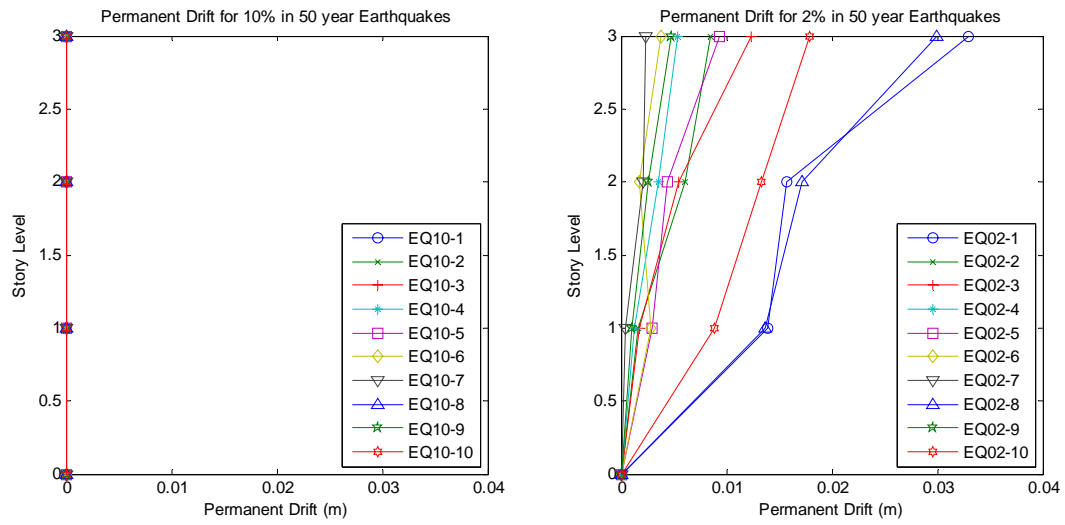
Figure 6.6 Permanent Drift for the Actively Controlled Structure (Placement B)

The maximum drift of each ground motion record is plotted against the record's demand as shown in Figure 6.7 in the probabilistic seismic demand model. The two best fit power law equations for Placement B are calculated as

$$Y_{P_{S_a}} = 4.226S_a^{0.9523}$$
$$R^2 = 0.995$$

(6.17)

$$Y_{P_{PGA}} = 8.7465PGA^{1.2816}$$
$$R^2 = 0.9497$$

(6.18)
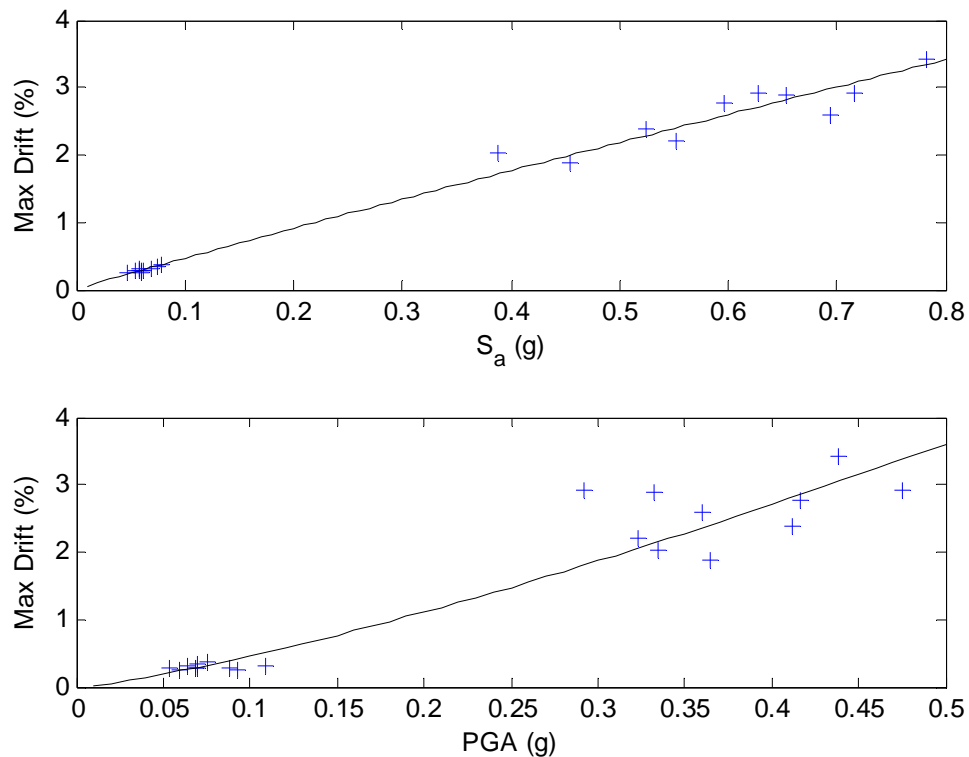
Figure 6.7 Probabilistic Seismic Demand Model for the

Actively Controlled Structure (Placement B)

The fragility curves for active controlled placement B is plotted in Figure 6.8b using spectral acceleration as the intensity measure for the three limit states. The fragility curves for the original structure are also shown. At S_a=0.6g, adding only two devices in the frame reduces the probability of exceeding life safety limit state from 65% of the original structure to 53% of the passive controlled structure and reduces the collapse prevention limit state from 11% to 6%. Again Figure 6.8a provides a visual comparison of the intensity level to the probability of exceedance in 50 years for Memphis, TN although this power law fit curve may not be appropriate for other uses.
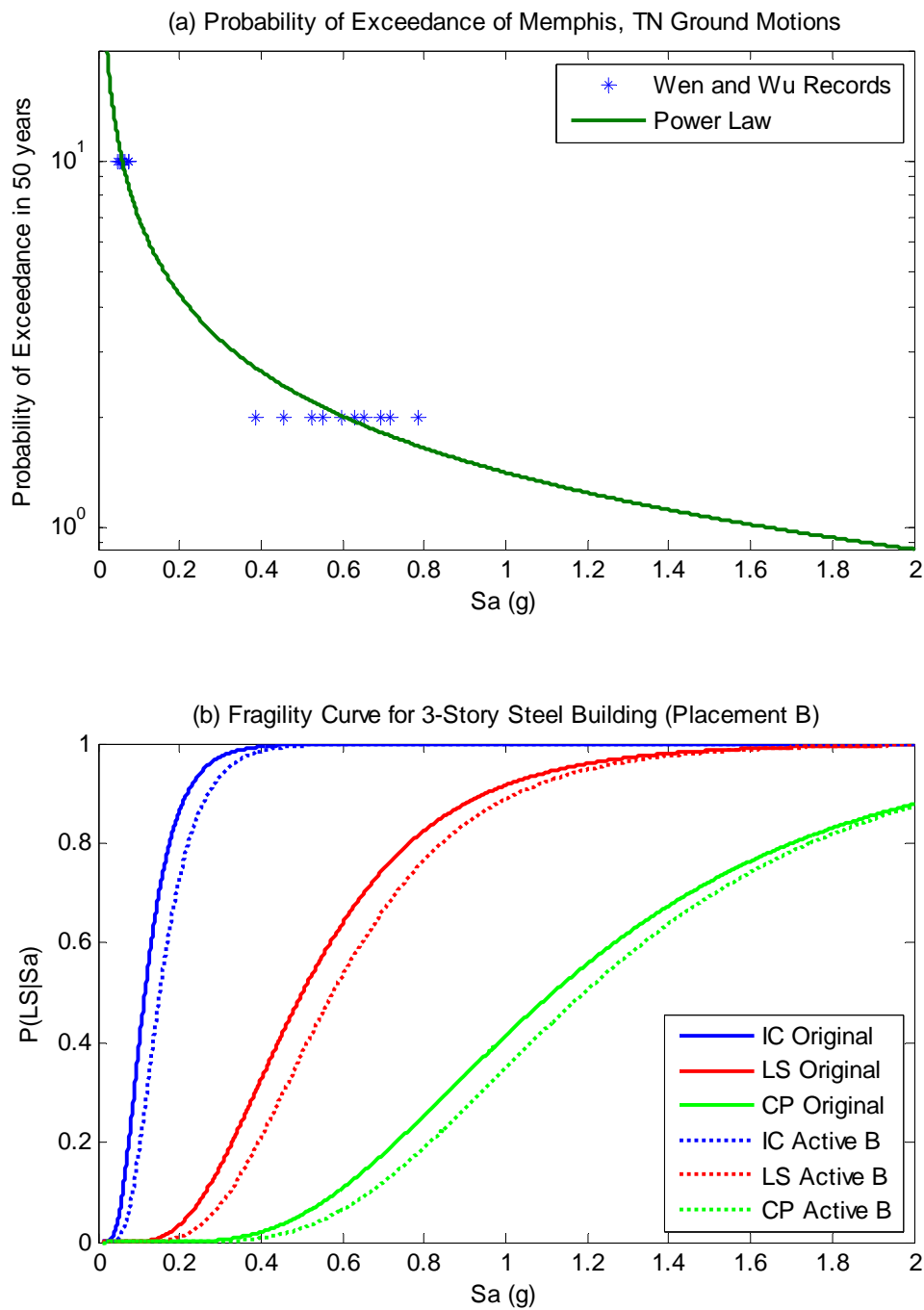
Figure 6.8 Fragility Curve of Actively Controlled Structure (Placement B)

6.2.3 Comparison of Active Placement A and Placement B

A comparison between the two device configurations is performed to investigate the differences in responses between six devices and two devices. Figure 6.9 shows the fragility curves for Placement A and Placement B of the actively controlled structure along with the original structure for the life safety limit state. Both active systems decrease the probability of failure. Placement A decreases the probability of exceeding the life safety limit state more so than Placement B, but one should expect a greater decrease in response when more devices are used.
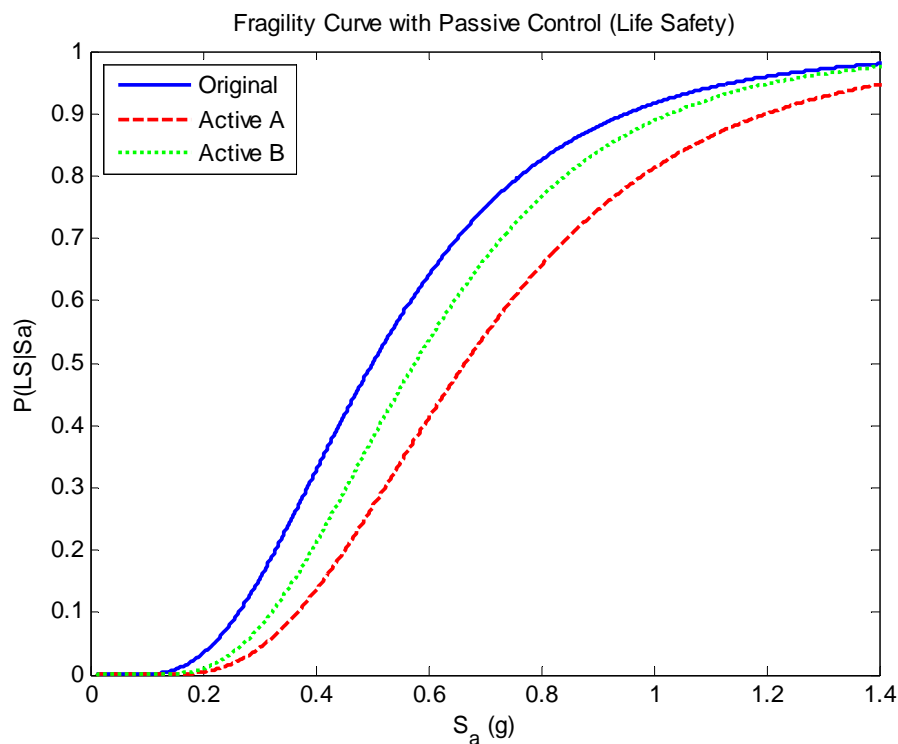
Figure 6.9 Comparison of Active Controlled Fragility Curves for Placement A and Placement B

6.3   Comparison of Passively and Actively Controlled Systems

An interest to this study is the comparison between the vulnerability between the active and passive systems. Figure 6.10 shows the comparison between the passive and active case for placement A. The passive and active cases are very similar with the passive case slightly achieving a lower fragility than the active case. Although one expects the active case to achieve better performance, the active controller could be achieving an optimal performance at the same level as the passive case.
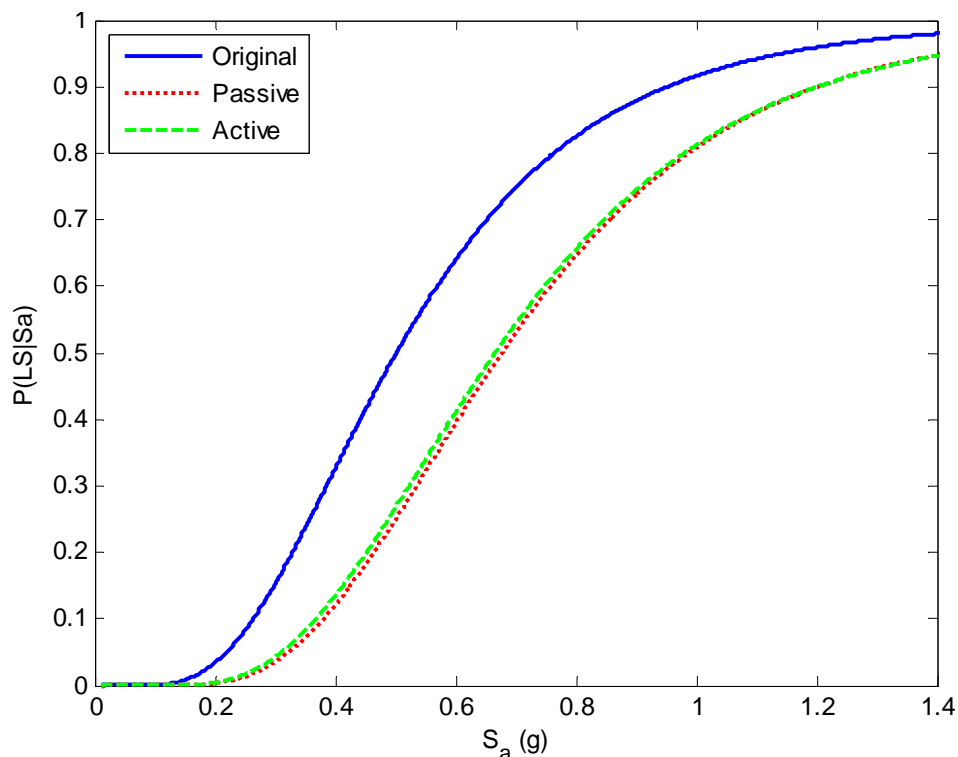
Figure 6.10 Comparisons of Fragility Curves for Placement A (Life Safety)

Figure 6.11 shows the comparison between the passive and active case for placement B. The fragility of the active device is shown to be improved at smaller intensity levels. When spectral acceleration is 0.3, the probabilities of failure of the actively controlled structure, the passively controlled structure, and the original structure are 7.5%, 12%,

and 15%, respectively. A crossover point occurs when the spectral acceleration is equal to 0.66g where the passively controlled structure has a lower fragility than the actively controlled structure. The probabilities of failure of the actively controlled structure, the passively controlled structure, and the original structure are 84%, 81%, and 88%, respectively when spectral acceleration is 0.9g. From the permanent drift figures, nonlinear behavior is shown at the 2% in 50 year exceedance level which is approximately when spectral acceleration is 0.6g. The active control algorithm uses the assumption of a linear system when the Kalman filter estimates the states of the system from the measured acceleration responses. When the structure experiences nonlinear behavior, the controller is unable to predict the states of the system effectively and therefore, the optimal force is no longer predicted accurately from a linear model.
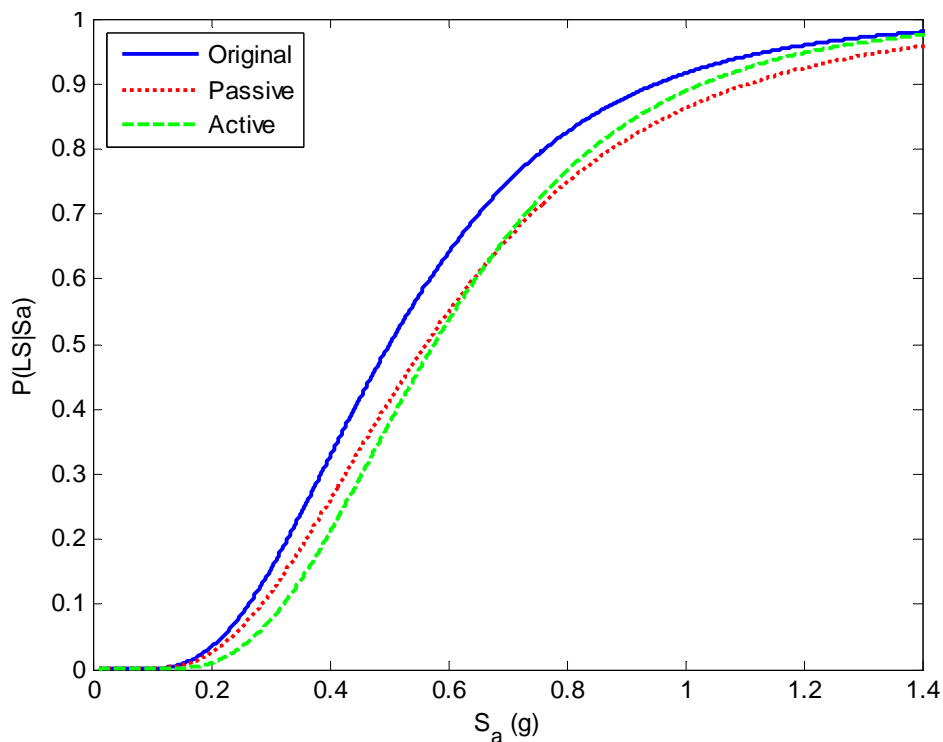
Figure 6.11 Comparisons of Fragility Curves for Placement B (Life Safety)

6.4   Summary

The development of fragility curves for active systems has been demonstrated. The addition of active devices has been shown to considerably reduce the vulnerability of the steel moment-resisting structure. Two device placements have been considered with one configuration chosen using engineering judgment and the other configuration found using optimal placement techniques. The optimal configuration (placement B) has a reduced number of devices, only two devices per frame compared to six devices of placement A. For the life safety limit state and the spectral acceleration is equal to 0.6g, the probability of failure of the original structure is 65% compared to 40% and 55% of active case A and active case B, respectively. The passive and active controlled systems are also compared. For placement A, the reduction of probability of failure from the original structure is approximately equal. However, for placement B, the active retrofit option reduces the probability of failure more than the passive case when the spectral acceleration is less than 0.66g. The active systems in this thesis were designed using a linear controller and linear devices so more potential is expected with complex systems. This thesis provides the tools to explore other control algorithms or devices in more complex systems.

Chapter 7

Conclusions

This thesis presents a methodology for developing fragility curves for controlled structures. A numerical example of a 3-story steel moment frame building is used to implement the procedure. Passive and active devices are considered in two different configurations. One device placement uses engineering judgment to place six devices, and the other placement configuration uses optimal placement to reduce the number of devices to two. Both passive and active systems reduced the vulnerability compared to the original system. Active control was found to surpass the passive case when optimal placement on considered with comparable force levels.

Background information on structural control and fragility curves is presented in Chapter 1. Chapter 2 proposes the five main steps to create a fragility curve as follows.

1. Appropriate ground motions are determined.
2. An analytical model of the controlled structural system is developed.
3. A probabilistic seismic demand model is calculated from time history responses.
4. The capacity of the elements is determined.
5. The fragility curve is analyzed using an appropriate equation.

Appropriate software was chosen to perform nonlinear time history analyses and demonstrate the proposed methodology. UI-SIMCOR is selected as the simulation coordinator to communicate between ZeusNL that models the stiffness of the structure and MATLAB that models the mass and damping and also calculates the control forces.

This process was first conducted on a three-story steel moment frame structure without retrofit to be able to compare the advantages of the control systems. The building model and the uncontrolled fragility for three limit states are presented in Chapter 3. Uncertainty in the fragility equation is investigated in Chapter 4.

Chapter 5 presents the change in fragility of a structure retrofitted with passive devices. Two device placements are considered: one chosen based on engineering judgment with six devices per moment resisting frame and the other using an optimal placement technique to reduce the number of devices to two per frame. Passive control is shown to reduce the vulnerability of the structure. For the life safety limit state and when the spectral acceleration is equal to 0.6g, the probability of failure of the original structure is 65% compared to 40% and 55% of the placement using engineering judgment and optimal placement, respectively. When six devices are used, a greater decrease in the probability of failure is shown even though the control effort is approximately equal. However, the additional cost of using three times the number of devices should be considered when comparing the reduction of vulnerability.

Fragility curves for the steel moment frame structure with active control are presented in Chapter 6. The two device placements determined in Chapter 4 are also used with active devices. Both active cases are designed using an H_2/LQG control law. Active control is also shown to reduce the vulnerability of the structure. For the life safety limit state and the spectral acceleration is 0.6g, the probability of failure of the original structure is 65% compared to 40% and 55% of active case A and active case B, respectively. Similar to the passively controlled systems, a greater decrease in the probability of failure is shown for the device configuration with more devices even though the control effort is approximately equal.

The passive and active control systems are also compared. The performance of the passive and active systems for placement A is very similar. However, the results for placement B are more interesting. The actively controlled case has a lower fragility at

smaller intensity levels, but a crossover point exists where the passive case has a lower fragility than the active case. An explanation for this phenomenon is that the active controller is designed for a linear system. Nonlinear behavior is shown from the permanent drifts from the 2% in 50 year exceedance records, which can be estimated when the spectral acceleration is 0.6g. The crossover point is at 0.66g and therefore, nonlinear behavior can be expected at the crossover point. As the nonlinear behavior becomes more prominent, the active control algorithm is not as effective in reducing the vulnerability because the Kalman filter estimates the states of the system assuming a linear system from the acceleration data.

7.1 Future Research

This thesis focused on the development of fragility relationships for controlled structures. The vulnerability of a structure with different types of control devices can easily be analyzed with a fragility curve. Multiple retrofit options including the addition of shear walls, braces, and column jackets have been studied by MAE Center researchers to reduce the vulnerability of the system. This study investigated the reduction of fragility with the addition of passive and active devices to the structural system compared to the original structure. The addition of these devices will be included in the MAE Center's database of retrofit options. The investigation into the fragility of other control classes is also of interest to engineers and decision-makers. The software used in this study was carefully chosen to have the capability of expanding this fragility curve methodology to include other control devices and algorithms which can be modeled within MATLAB including MR dampers or other semiactive devices. Hybrid systems or other systems implementing more than one type of device can also use the presented methodology to compare the vulnerability of different controlled structures. This thesis provides the tools to expand to complex control systems and more potential could be expected with those systems.

References

Abrams, D. P., A. S. Elnashai, and J. E. Beavers (2002), "A New Engineering Paradigm: Consequence-Based Engineering," Linbeck Lecture Series in Earthquake Engineering: Challenges of the New Millennium, University of Notre Dame's Linbeck Distinguished Lecture Series, Notre Dame, IN..

AISC (2001), *Manual of Steel Construction - Load and Resistance Factor Design* (LRFD), Third Edition, American Institute of Steel Construction (AISC), Chicago, Illinois.

Bai J.W. (2004), *Seismic fragility and retrofitting for a reinforced concrete flat-slab structure*. Masters Thesis. Texas A&M University, College Station, TX.

Bai J.W., M. Hueste and P. Gardoni (2006) "A Probabilistic Framework for the Assessment of Stuctural Losses due to Seismic Events" In preparation for publication, June 30, 2006.

Baker, J.W. and C.A. Cornell (2006) "Which Spectral Acceleration Are You Using?" EERI *Earthquake Spectra*, 22(2), pp. 293-312.

Borcherdt R.D. and G. Glassmoyer (1992) "On the characteristics of local geology and their influence on ground motions generated by the Loma Prieta earthquake in the San Francisco Bay region, California," *Bulletin of the Seismology Society of America*, 82(2), pp. 603-641.

Elnashai, A. S., Papanikolaou, V., and Lee, D. (2002), "Zeus NL – A System for Inelastic Analysis of Structures," Mid-America Earthquake Center, University of Illinois at Urbana-Champaign, Program Release Sept. 2002.

FEMA (2000), Prestandard and Commentary for the Seismic Rehabilitation of Buildings (*FEMA 356*), prepared by the American Society of Civil Engineers for the Federal Emergency Management Agency, Reston, VA.

Frankel A.D., M.D. Petersen, C.S. Mueller, K.M. Haller, R.L. Wheeler, E.V. Leyendecker, R.L. Wesson, S.C. Harmsen, C.H. Cramer, D.M. Perkins, and K.S. Rukstales (2002) "Documentation for the 2002 Update of the National Seismic Hazard Maps," USGS Open-File Report 02-420.

Giulio, G.D., R.M. Azzara, G. Cultrera, M.S. Giammarinaro, P. Vallone, and A. Rovelli (2005) "Effect of Local Geology on Ground Motion in the City of Palermo, Italy, as

Inferred from Aftershocks of the 6 September 2002 Mw 5.9 Earthquake," Bulletin of the Seismological Society of America, 95(6), pp. 2328-2341.

Hudson D.E. (1972), "Local distribution of strong earthquake ground motions," Bulletin of the Seismological Society of America, 62(6), pp. 1765-1786.

Dyke, S.J., Spencer Jr., B.F., Quast, P. and Sain, M.K. (1995), "Role of Control-Structure Interaction in Protective System Design," *J. of Engrg. Mech, ASCE*, 121(2), pp. 322–38.

Dyke, S.J., B.F. Spencer, Jr., M.K. Sain and J.D. Carlson (1996a), "Modeling and Control of Magnetorheological Dampers for Seismic Response Reduction," *Smart Materials and Structures,* Vol. 5, pp. 565–575.

Dyke, S.J. B.F. Spencer, P. Quest, M.K. Sain, D.C. Kaspari Jr, and T.T. Soong (1996b) "Acceleration Feedback Control for MDOF Structures," *Journal of Engineering Mechanics*, 122(9), pp. 907-918.

Dyke, S.J., Spencer Jr., B.F., Sain, M.K. and Carlson, J.D. (1998), "An Experimental Study of MR Dampers for Seismic Protection," *Smart Materials and Structures: Special Issue on Large Civil Structures*, Vol. 7, pp. 693–703.

Gawronski, W. K. (1998), *Dynamics and Control of Structures: A Modal Approach*, Mechanical Engineering Series, Springer-Verlag New York, Inc.

Gilani, A., Miyamoto, H.K., and Kohagura, T. (2006), "Application of Fluid Viscous Dampers in Seismic Design and Rehabilitation of Steel Frame Essential Facilities," Proceedings of the 8th U.S. National Conference on Earthquake Engineering, San Francisco, California, April 2006.

Jansen, L.M. and Dyke, S.J. (2000), "Semi-Active Control Strategies for MR Dampers: A Comparative Study," *J. Engrg. Mechanics*, ASCE, 126(8), pp. 795–803.

Jeong, S.H. and A.S. Elnashai (2004) "Parameterized Vulnerability Functions for As-built and Retrofitted Structures," Proceedings of the International Workshop on Performance-Based Seismic Design, Bled, Slovenia, June 2004.

Kim, S.H. and M. Shinozuka (2004), **"**Development of fragility curves of bridges retrofitted by column jacketing," *Probabilistic Engineering Mechanics*, 19(1-2), pp. 105-112.

Kitagawa Y. and S. Akutagawa (2006), "Adaptive Structural Control Method as a Smart Structural System," Proceedings of the 8th U.S. National Conference on Earthquake Engineering, San Francisco, California, April 2006.

Kwon, O., N. Nakata, A. Elnashai, B. Spencer (2005), "Technical Note: A Framework for Multi-Site Distributed Simulation and Application to Complex Structural Systems," *Journal of Earthquake Engineering*, 9(5), pp. 741-753.

Lew, H.S. and Kunnath, S.K. (2002) Assessment of Structural Systems Evaluation Methods Based on Local Seismic Demands. *Innovations in Design with Emphasis on Seismic, Wind and Environmental Loading, Special Publication SP-209-42*, American Concrete Institute, Farmington, Michigan, pp.771-790

MATLAB (1997), The Math Works, Inc., Natick, Massachusetts.

Ohtori, Y., R. E. Christenson, B. F. Spencer, and S. J. Dyke (2004), "Benchmark Control Problems for Seismically Excited Nonlinear Buildings," *Journal of Engineering Mechanics*, 130(4), pp. 366-385.

Padgett, J. and R DesRoches (2006), "Retrofitted Bridge Fragility Curves for Assessing the Impact of Retrofit on Bridge System Performance," Proceedings of the ASCE Structures Congress , St. Louis , MO. , April 2006.

SAC Steel Project. (1994), Technical Office, Richmond, Calif. 94804-4698. <http.//www.sacsteel.org/>.

Shing, P.S. and M.T. Vannan (1991) "Implicit Time Integration for Pseudodynamic Tests: Convergence and Energy Dissipation," *Earthquake Engineering and Structural Dyanamics*, Vol. 20, pp. 809-819.

Shinozuka, M., M.Q. Feng, J. Lee, and T. Naganuma (2000a), "Statistical Analysis of Fragility Curves," *Journal of Engineering Mechanics*, 126(12), pp. 1224-1231.

Shinozuka, M., M.Q. Feng, H.K. Kim and S.H. Kim (2000b), "Nonlinear Static Procedure for Fragility Curve Development," *Journal of Engineering Mechanics*, 126(12), pp. 1287-1295.

Shooshtari, M. and M. Saatcioglu (2006), "Active Seismic Control of Reinforced Concrete Frames," Proceedings of the 8th U.S. National Conference on Earthquake Engineering, San Francisco, California, April 2006.

Singhal, A. and A.S. Kiremidjian (1996), "Method for probabilistic evaluation of seismic structural damage," *Journal of Structural Division*, ASCE, 122(12), pp. 1459-1467.

Singhal, A. and A.S. Kiremidjian (1998), "Bayesian Updating for Fragilities with Application to RC Frames," *Journal of Structural Engineering*, 124(8), pp. 922-929.

Spencer, Jr. B.F., Dyke, S.J., and Deoskar, H.S. (1998), "Benchmark Problems in Structural Control: Part 1-Active Mass Driver System." *Earthquake Engr & Struc Dyn: Special Issue on the Benchmark Structural Control Comparison*, 27, pp. 1127-1139.

Spencer, Jr. B.F., J. Suhardjo, and M. K. Sain. (1994) "Frequency domain optimal control strategies for aseismic protection." *Journal of Engineering Mechanics*, 120(1), pp. 135-159.

Stover, C.W. and J. L. Coffman (1993) "Seismicity of the United States," U.S. Geological Survey Professional Paper 1527, Retrieved from http://www.usgs.gov.

USGS (2006) "Historic Earthquakes," U.S. Geological Survey, Retrieved from http://earthquake.usgs.gov.

Wang Y. (2006), *Control Strategies for 3-D Smart Base Isolation Systems Using Modal and Nodal Approaches*. Doctoral Dissertation. Washington University, St. Louis, Missouri.

Wen, Y.K., B.R. Ellingwood, D. Veneziano, and J. Bracci (2003) "Uncertainty Modeling in Earthquake Engineering," MAE Center Project FD-2 Report, Mid-America Earthquake Center, University of Illinois at Urbana-Champaign.

Wen. Y. K. and Ellingwood, B. R. (2005), "The Role of Fragility Assessment in Consequence-Based Engineering," EERI *Earthquake Spectra*, 21(3), pp. 861-877.

Wen Y.K., Ellingwood, B.R. and Bracci, J. (2004), "Vulnerability Function Framework for Consequence-based Engineering," MAE Center Project DS-4 Report, Mid-America Earthquake Center, University of Illinois at Urbana-Champaign.

Wen, Y.K. and Wu, C.L. (2001), "Uniform hazard ground motions for mid-America cities," *Earthquake Spectra*, 17(2), pp. 359-384.

Williams S. (2004), *Fault-Tolerant Control Design for Smart Damping Systems*. Masters Thesis. Washington University, St. Louis, Missouri.

Yao, J.T.P. (1972) "Concept of Structural Control," *Journal of the Structural Division*, 98(7), pp. 1567-1572.

Yi, F. and S.J. Dyke (2000) "Structural control systems: performance assessment" Proceedings from American Control Conference, Chicago, IL.

Yoshida, O. and Dyke, S.J. (2004), "Seismic Control of a Nonlinear Benchmark Building Using Smart Dampers," *Journal of Engineering Mechanics: Special Issue on Benchmark Control Problems*, 130(4), pp. 386–392.

Vita

Ellen D. Taylor

Date of Birth	May 18, 1982
Place of Birth	San Antonio, Texas
Degrees	B.S. Engineering with a Civil Specialty with Honors, Colorado School of Mines, May 2004
	MS. Civil Engineering, Washington University in St. Louis, May 2007
Professional Societies	American Society of Civil Engineers Earthquake Engineering Research Institute Mid-America Earthquake Center
Publications	A. Hurd, E. Taylor, S.J. Dyke and K. Truman. "Structural Engineering in the Middle School Classroom: Building a Foundation in Math and Science." *Proceedings, International Conference on Engineering Education*, San Juan, Puerto Rico, July 24-28, 2006.
	E. Taylor and S.J. Dyke. "Development of Fragility Relationships for Smart Structures." *Proceedings, 4th World Conference on Structural Control and Monitoring*, San Diego, California July 11-13, 2006.
	S.J. Dyke, Y. Wang, E. Taylor. "Seismic Response Modification Using Innovative Damping Devices." *Proceedings of the 3rd Colombian Conference on Earthquake Engineering*, Cali, Colombia, November 16-18, 2005.
	E. Taylor. "Vibration Control for Two Dynamically Similar Structures." *Proceedings of the Research Experiences for Undergraduates in Japan Symposium*, Tokyo, Japan, August 3, 2003.

May 2007

Short Title: Fragility Curves   **Taylor, M.S. 2007**